Three dimensional homogenization of masonry structures with building blocks of finite strength: A closed form strength domain

Ioannis Stefanou, Karam Sab, Jean-Vivien Heck

Three dimensional homogenization of masonry structures with building blocks of finite strength: A closed form strength domain

Ioannis Stefanou[a,1], *Karam Sab*[a], *Jean-Vivien Heck*[b]

[a] *Université Paris-Est, Laboratoire Navier (UMR 8205), CNRS, ENPC, IFSTTAR, F-77455 Marne-la-Vallée cedex 2, France*

[b] *Centre Scientifique et Technique du Bâtiment (CSTB), 84, avenue Jean-Jaurès, Champs sur Marne, 77447 Marne-la-Vallée cedex 2, France*

Abstract: The present paper provides a straightforward methodology for the estimation in closed form of the overall strength domain of an in-plane loaded masonry wall by accounting for the failure of its bricks. The determination of the overall strength domain was based on a rigorous definition of the microstructure in three-dimensions, on convex analysis and on the kinematical approach in the frame of limit analysis theory. No plane stress or plane strain assumption is a priori made. The formulation allowed distinguishing the yield surfaces that account for the failure of the joints and the yield surfaces that account for the failure of the building blocks. The validity and the efficiency of the derived analytical strength domain were investigated by means of numerical homogenization and experimental evidence. The proposed strength domain can be used in limit analysis approaches, in finite element simulations and for

[1] Corresponding author : Ioannis STEFANOU, MSA – Navier Laboratory
Ecole des Ponts Paris Tech, 6-8 Av. Blaise Pascal, Cité Descartes Champs sur Marne, 77455 MARNE LA VALLEE Cedex 2 FRANCE
Email: Ioannis.Stefanou@enpc.fr
Phone: +33 (0) 1 64 15 34 77
Fax: +33 (0) 1 64 15 37 41

calibrating existing phenomenological models for masonry structures based on the micromechanical properties and the geometry of the bricks and the mortar.

Keywords: *masonry; failure; homogenization; microstructure; multisurface plasticity; limit analysis*

1 Introduction

The failure of masonry structures can be studied either by continuum or discrete type models (cf. macro-modeling and micro-modeling Lourenço, 1996). The latter consider the masonry as an assemblage of blocks (bricks) with explicitly defined geometry and joints (interfaces), while the former consider the masonry as a continuum medium. Continuum models are based on either simplified analytical approaches or on homogenization techniques. Each approach has advantages and disadvantages that are related to the required computational effort and the degree of accuracy of the obtained results. Due to the heterogeneous nature of masonry structures, discrete type approaches seem to be the physical starting point for the modeling of the mechanical behavior of such kind of structures. Nevertheless, because of the difficulty in determining the exact mechanical parameters at the microlevel and the considerable computational cost of discrete type approaches, continuum approaches continue to attract the interest of many researchers. In spite of the several limitations of continuum mechanics for modeling such kind of heterogeneous systems (at least for classical Cauchy continua (Zucchini & Lourenço, 2007)) the main reason for using continuum models is that they offer a certain degree of abstraction and allow to up-scale the micromechanical characteristics to the macroscale, i.e. to the scale of the structure.

A considerable number of continuum models for masonry already exist in the literature. Among others we refer to the works of Heyman (1966), Page (1978), Livesley (1978), Alpa & Monetto (1994), Pande et al. (1989), Lotfi & Shing (1991), Pietruszczak & Niu (1992),

Cecchi & Sab (2002), Zucchini & Lourenço (2002, 2007), Milani et al. (2006a, 2006b) in the frame of classical contimmum theory and to Sulem & Mühlhaus (1997), Masiani & Trovalusci (1996), Stefanou et al. (2008, 2010), Salerno & de Felice (2009), Addessi, Sacco, & Paolone (2010), Pau & Trovalusci (2012), Trovalusci & Pau (2013) for continuum models using higher order continuum theories. For a comprehensive review of various continuum models we refer to the article of Lourenço et al. (2007). As a general remark one could state that most of the available continuum models describe the elastic linear behavior of brickwork by proposing even closed form expressions for the elastic moduli. On the contrary, the inelastic behavior of masonry is studied in fewer works through non-linear homogenization approaches that in most of the cases are based on extensive numerical simulations.

Homogenization theory (Bakhvalov & Panasenko, 1989; Bensoussan, Lions, & Papanicolaou, 1978) has been applied in order to derive the effective linear elastic constitutive parameters of an equivalent Cauchy continuum based on the microstructure of the masonry. Based on a kinematic limit analysis homogenization approach and under plane stress conditions, de Buhan and de Felice (1997) have derived in closed-form the strength domain of an in-plane loaded periodic brickwork consisting of infinitely resistant (elastic) bricks connected with Coulomb interfaces. The derived yield criteria consist an upper bound of the strength domain. Considering a polynomial distribution of the stresses and a two dimensional stress field (imposed plane stress conditions), Milani et al. (2006a, 2006b) proposed a homogenization scheme in order to determine a lower bound of the strength domain of masonry. The aforementioned homogenization approach allowed to consider different yield criteria for bricks and mortar. Massart et al. (2005, 2007) and Zucchini & Lourenço (2002, 2004, 2007) considered additionally the brittle behavior of bricks and mortar in the frame of damage mechanics theory. Nevertheless, the strength domain in the abovementioned approaches does not have an analytical, closed form expression.

The present paper focuses on providing a straightforward methodology for the analytical, closed-form estimation of the overall strength domain of an in-plane loaded masonry wall made of bricks of finite strength connected with frictional interfaces. The determination of the overall in-plane strength domain was based on a kinematic limit analysis approach in three dimensions (3D). It has to be emphasized that the common plane stress or the plane strain or the generalized plane strain assumptions were avoided (these terms are used as defined in Saada (1974)). According to Anthoine (1997), the aforementioned states of plane deformation might have little influence on the macroscopic elastic behavior of masonry (Addessi & Sacco, 2014; Mistler, Anthoine, & Butenweg, 2007), but may significantly affect its non-linear response (at least for materials described in the damage mechanics framework which was used in Anthoine, 1997). Therefore, the three dimensional kinematic approach followed here permits the generalization and extension of the results of de Buhan and de Felice (1997) by taking into account the out-of-plane deformations of the masonry due to in-plane loading and by considering a finite strength for the blocks. Depending on the constitutive behavior of the masonry units and of the joints an analytical closed form expression for the masonry strength domain is determined.

The kinematic approach leads, in principle, to an upper bound of the exact strength domain of the system (cf. Salençon, 1990). Therefore, the accuracy of the abovementioned analytically derived strength domain was investigated through numerical homogenization of the 3D unit cell and it was compared to the experimental results of Page (1981, 1983). The effect of the thickness of the joints was explored and its influence was found to be quite limited for thin joints.

The paper has the following structure. In section 2 the overall in-plane strength domain of a running bond masonry wall is determined based on a kinematic limit analysis approach and using a three-dimensional stress and kinematic field. In this section the formulation is

general, no plane stress assumption is made and not any particular material is chosen for the interfaces and the building blocks. The masonry wall is treated as a thin plate with a periodic microstructure of finite thickness. In section 3, the derived strength domain is compared to the strength domain found by numerical homogenization. The interfaces and the blocks are considered to obey to a Drucker-Prager criterion in order to avoid possible numerical problems. Three yield surfaces that account for the failure of the joints, and one yield surface that accounts for the failure of the units are expressed in closed form. Their intersection in the stress space forms the in-plane strength domain, which is compared with the strength domain derived numerically. It is shown that the numerical and the analytical results coincide in the majority of biaxial load configurations tested. Nevertheless, under some biaxial load conditions and for thick joints the resistance of the masonry is somehow overestimated. Finally, in section 4 the analytically derived strength domain is compared to the experimental results of Page (1981; 1983) by adopting a Coulomb criterion both for the interfaces and the blocks. The comparison is quite satisfactory.

The derived analytical strength domain can be used in limit analyses in order to assess the ultimate failure load, in finite element simulations (e.g. de Felice, Amorosi, & Malena, 2009) and due to its simple closed-form expression can be used for the calibration of existing phenomenological models (e.g. Ottosen, 1977; Syrmakezis & Asteris, 2001).

2 Three dimensional homogenization of masonry walls

Homogenization theory is applied in order to determine the overall in-plane strength domain of a running bond masonry wall. A kinematic limit analysis approach is followed using a three-dimensional stress and kinematic field. It is worth emphasizing that unlike similar existing homogenization approaches for masonry (e.g. de Buhan & de Felice, 1997; Milani et al., 2006), no plane stress conditions are a priori assumed and the problem is treated in three

dimensions. The reason is that the stress state in the mortar cannot be described precisely either by plane stress or plane strain conditions. In particular, one can imagine that when the joints are very thin the mortar is in plane strain conditions as the masonry units constrain its deformation. On the contrary, when the joints are very thick, the influence of the units on the deformation of the mortar is small and one can consider that the mortar deforms rather under plane stress conditions. Following the definitions of Saada (1974), in the absence of lateral loadings, a masonry wall is in a generalized plane stress state, i.e. the stress is zero at its lateral sides, but not in every point in its thickness (cf. plane stress conditions). The influence of plane stress or of generalized plane strain conditions is well-known (Anthoine, 1997; Mistler et al., 2007) and in the non-elastic regime, different states of plane deformation can have important impact. Generalized plane strain and simplified 3D approximations give better results as far it concerns the resistance of masonry (Addessi & Sacco, 2014; Anthoine, 1995). The plane stress assumption is inadequate for thick masonry walls (Anthoine, 1997). To overcome these issues a three dimensional kinematic and stress field is taken into account and the masonry wall is considered as a plate of finite thickness.

Let the heterogeneous plate occupy the domain $\Omega = \omega \times \left]-\frac{t}{2},\frac{t}{2}\right[$ where $\omega \subset \mathbb{R}^2$ is the middle surface (middle plane) and t the thickness of the plate. The plate consists of an elementary cell that it is periodically repeated in directions 1 and 2 (see Figure 1) and its size is small in comparison to the size of the total structure. The elementary unit cell is denoted by the domain $Y = A \times \left]-\frac{t}{2},\frac{t}{2}\right[$, where $A \subset \mathbb{R}^2$. The boundary ∂Y of Y is decomposed into three parts, $\partial Y = \partial Y_l \cup \partial Y_3^+ \cup \partial Y_3^-$, with $\partial Y_3^{\pm} = \left\{\pm\frac{t}{2}\right\}$.

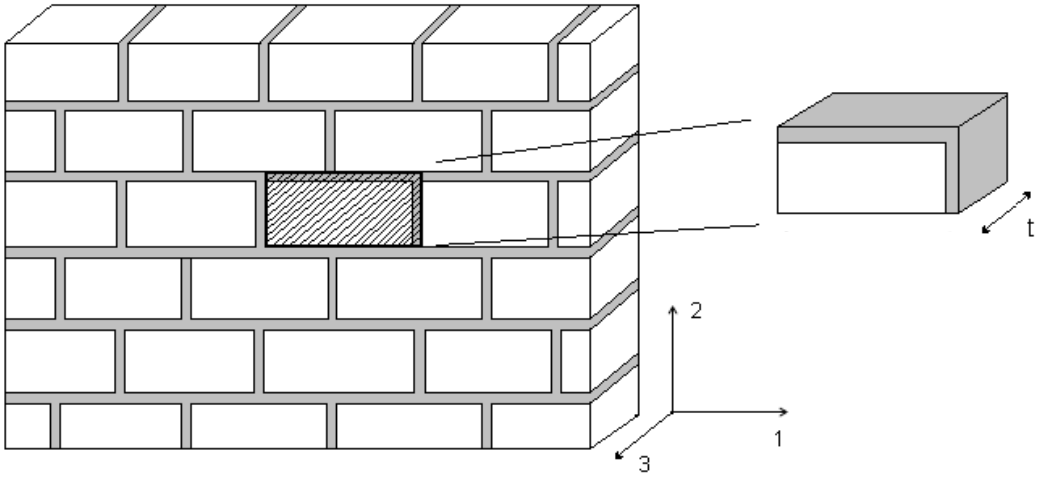

Figure 1. The running bond masonry geometry and the unit cell considered herein.

We assume that the strength of the material at every point $\mathbf{y} \in Y$ is defined by a convex closed domain $G(\mathbf{y})$, such that $\boldsymbol{\sigma} \in G$, with $\boldsymbol{\sigma} = (\sigma_{ij})$ the stress tensor and $i, j = 1,2,3$. No plane stress assumption is made and therefore σ_{13}, σ_{23} and σ_{33} are not zero. Such a domain is uniquely defined by a positive homogeneous function of degree one, which is called support function and it is defined as:

$$\pi(\mathbf{d}) = sup\{\boldsymbol{\sigma} : \mathbf{d}, \boldsymbol{\sigma} \in G\} \Leftrightarrow G = \{\boldsymbol{\sigma} | \boldsymbol{\sigma} : \mathbf{d} \le \pi(\mathbf{d}), \forall \mathbf{d}\} \tag{1}$$

where $\mathbf{d} = (d_{ij})$ denotes a strain rate tensor and ':' denotes the double contraction.

If the thickness, t, of the 3D-structure (i.e. the thickness of the masonry wall) is comparable to the size of the unit cell (i.e. the periodic masonry cell), but it is very small compared to the overall size of the structure, ω, then, as it was proposed by Sab (2003) and Dallot & Sab (2008a, 2008b), the periodic structure can be modeled as a homogeneous Love-Kirchhoff plate. Let $\mathbf{N} = (N_{\alpha\beta}(x_1, x_2))$ be the macroscopic in-plane (membrane) stress field resultants for the homogenized plate with $(x_1, x_2) \in \omega$ and $\alpha, \beta = 1,2$, $\mathbf{M} = (M_{\alpha\beta}(x_1, x_2))$ the

macroscopic out-of-plane (flexural) stress field resultants, $\mathbf{D}=\left(D_{\alpha\beta}\left(x_1,x_2\right)\right)$ the in-plane strain rate field, $\boldsymbol{\chi}=\left(\chi_{\alpha\beta}\left(x_1,x_2\right)\right)$ the out-of-plane (curvature) strain rate field and $\mathbf{V}=\left(V_i\left(x_1,x_2\right)\right)$ the plate velocity field. The macroscopic rate fields are related to the macroscopic virtual velocity field components as follows: $D_{\alpha\beta}=\frac{1}{2}\left(V_{\alpha,\beta}+V_{\beta,\alpha}\right)$ and $\chi_{\alpha\beta}=-V_{3,\alpha\beta}$. Then the convex strength domain of the homogenized plate, G_p^{hom}, can be determined by solving an auxiliary limit analysis problem over the unit cell, Y .

2.1 Definition of the homogenized plate strength domain

For every $\left(\mathbf{N},\mathbf{M}\right)$ the set $SA\left(\mathbf{N},\mathbf{M}\right)$ of statically admissible Y -periodic 3D stress field $\boldsymbol{\sigma}$ of the unit cell Y is defined by:

$$SA(\mathbf{N},\mathbf{M})=\left\{\begin{array}{c}\boldsymbol{\sigma}\mid N_{\alpha\beta}=t\left\langle\sigma_{\alpha\beta}\right\rangle, M_{\alpha\beta}=t\left\langle y_3\sigma_{\alpha\beta}\right\rangle\\ div\,\boldsymbol{\sigma}=0 \text{ on } Y\\ \boldsymbol{\sigma}\cdot\mathbf{n} \text{ skew-periodic on } \partial Y_l\\ \boldsymbol{\sigma}\cdot\mathbf{e}_3=0 \text{ on } \partial Y_3^{\pm}\end{array}\right\} \tag{2}$$

where $\langle\cdot\rangle$ is the volume average operator on Y .

The homogenized strength domain, G_p^{hom}, is defined as the set of the generalized stresses $\left(\mathbf{N},\mathbf{M}\right)$ such that there is a 3D stress field $\boldsymbol{\sigma}$ in $SA\left(\mathbf{N},\mathbf{M}\right)$ with $\boldsymbol{\sigma}\left(\mathbf{y}\right)\in G\left(\mathbf{y}\right)$ for all $\mathbf{y}$ in Y , i.e. $G_p^{hom}=\left\{\left(\mathbf{N},\mathbf{M}\right)\mid\exists\sigma\in SA\left(\mathbf{N},\mathbf{M}\right),\sigma\left(\mathbf{y}\right)\in G\left(\mathbf{y}\right),\forall\mathbf{y}\in Y\right\}$.

For every $\left(\mathbf{D},\boldsymbol{\chi}\right)$ the set of the kinematically admissible velocity fields of the unit cell, $\mathbf{v}=\left(v_i\right)$, is defined as follows:

$$KA\left(\mathbf{D},\boldsymbol{\chi}\right)=\left\{\mathbf{v}\mid\nabla\otimes^s\mathbf{v}=\tilde{\mathbf{D}}+y_3\tilde{\boldsymbol{\chi}}+\nabla\otimes^s\mathbf{u}^{per},\mathbf{u}^{per}\,Y-\text{periodic}\right\} \tag{3}$$

where $\nabla\otimes^s \mathbf{v}$ is the symmetric part of the gradient operator and $\tilde{D}_{\alpha\beta} = D_{\alpha\beta}$, $\tilde{D}_{i3} = 0$, $\tilde{\chi}_{\alpha\beta} = \chi_{\alpha\beta}$, $\tilde{\chi}_{i3} = 0$.

The sets $SA(\mathbf{N},\mathbf{M})$ and $KA(\mathbf{D},\boldsymbol{\chi})$ are conjugate in virtual power on the unit cell, i.e. $\forall\boldsymbol{\sigma} \in SA(\mathbf{N},\mathbf{M})$ and $\forall\mathbf{v} \in KA(\mathbf{D},\boldsymbol{\chi})$, $\mathbf{N}:\mathbf{D} + \mathbf{M}:\boldsymbol{\chi} = t\left\langle \boldsymbol{\sigma} : \left(\nabla\otimes^s \mathbf{v}\right)\right\rangle$. Therefore, G_p^{hom} (Sab, 2003; Salençon, 1990b; Suquet, 1983) becomes:

$$\pi_p^{\hom}(\mathbf{D},\boldsymbol{\chi}) = \inf_{\mathbf{v}\in KA(\mathbf{D},\boldsymbol{\chi})} \left\{ t\left\langle \pi\left(\nabla\otimes^s \mathbf{v}\right)\right\rangle\right\} \tag{4}$$

2.2 Definition of the homogenized in-plane strength domain

The in-plane strength domain is defined as the set, G^{Σ}, of the symmetric second order in-plane stress tensors $\boldsymbol{\Sigma} = \left(\Sigma_{\alpha\beta}\right)$ defined by $\boldsymbol{\Sigma} \in G^{\Sigma}$ or equivalently $t\boldsymbol{\Sigma} \in G^N$. G^N is the intersection of G_p^{hom} with the subspace $(\mathbf{N},\mathbf{M} = 0)$ or equivalently, as it will be shown below, the projection of G_p^{hom} to the subspace $(\mathbf{N},\mathbf{M} = 0)$, i.e. $G^N = \left\{\mathbf{N} \mid \exists\mathbf{M}, (\mathbf{N},\mathbf{M}) \in G_p^{\hom}\right\}$. Its corresponding support function is $\pi^N(\mathbf{D}) = \pi_p^{\hom}(\mathbf{D},\mathbf{0})$. Hence, according to the static definition of $G_p^{\hom}$, $\boldsymbol{\Sigma} \in G^{\Sigma}$ if there exists a Y-periodic stress field $\boldsymbol{\sigma} = \left(\sigma_{ij}\right)$ of the 3D unit cell verifying:

$$\begin{gathered} \boldsymbol{\sigma}(\mathbf{y}) \in G(\mathbf{y}),\ \forall\mathbf{y} \in Y \\ \left\langle \sigma_{\alpha\beta}\right\rangle = \Sigma_{\alpha\beta} \\ div\,\boldsymbol{\sigma} = 0 \text{ on } Y \\ \boldsymbol{\sigma}\cdot\mathbf{n} \text{ skew-periodic on } \partial Y_l \\ \boldsymbol{\sigma}\cdot\mathbf{e}_3 = 0 \text{ on } \partial Y_3^{\pm} \end{gathered} \tag{5}$$

Using Eq.(5)c and the boundary conditions, it can be shown that the average of the out-of-plane components, $\left\langle\sigma_{i3}\right\rangle$, of a stress tensor $\boldsymbol{\sigma}$ satisfying Eq.(5) are zero. It is worth

mentioning that $\boldsymbol{\sigma}$ is not a plane stress field but a generalized plane stress field according to the definition of Saada (1974). Eqs. (5) define the numerical homogenization problem solved in section 3.2 in order to validate the upper bound of the strength domain derived in sections 2.4 and 2.5.

The kinematic definition of G^{Σ} is as follows:

$$G^{\Sigma} = \left\{ \boldsymbol{\Sigma} = \left(\Sigma_{\alpha\beta} \right) \mid \boldsymbol{\Sigma} : \mathbf{D} \le \pi^{\Sigma}\left(\mathbf{D} \right), \forall \mathbf{D} = \left(D_{\alpha\beta} \right) \right\} \tag{6}$$

where π^{Σ} is the support function of G^{Σ} and it is given by:

$$\pi^{\Sigma}\left(\mathbf{D} \right) = t^{-1}\pi_p^{\hom}\left(\mathbf{D}, \mathbf{0} \right) = \inf_{\mathbf{v} \in KA(\mathbf{D},0)} \left\{ \left\langle \pi\left(\nabla \otimes^s \mathbf{v} \right) \right\rangle \right\} \tag{7}$$

In the general case of $\mathbf{v} \in KA\left(\mathbf{D}, \mathbf{0} \right)$ the corresponding $\mathbf{u}^{per}\left(y_1, y_2, y_3 \right)$ in Eq.(3) has three components ($u_3 \neq 0$) and it is Y -periodic. Therefore, the average out-of-plane components of $\mathbf{d} = \nabla \otimes^s \mathbf{v}$ for $\mathbf{v} \in KA\left(D, 0 \right)$ are not zero.

In other words, $\left\langle d_{\alpha\beta} \right\rangle = D_{\alpha\beta}$ and $\left\langle d_{i3} \right\rangle \neq 0$ in the general case. In this sense the 3D unit cell problems described in Eqs.(5) and (7) cannot be considered as plane stress or plane strain problems.

A periodic plate is *symmetric* if one can extract a centro-symmetric unit cell ($\mathbf{y} \in Y \Leftrightarrow -\mathbf{y} \in Y$) such that $G\left(\mathbf{y} \right) = G\left(-\mathbf{y} \right)$ $\forall \mathbf{y} \in Y$. In this case G^N coincides with the intersection of $G_p^{\hom}$ with the subspace $\left(\mathbf{N}, \mathbf{M} = \mathbf{0} \right)$. This means that the conditions $\left\langle y_3 \sigma_{\alpha\beta} \right\rangle = 0$ can be added to the static definition of G^{Σ} (see Eq.(5)) and that the infimum in Eq.(7) can be taken over all $\mathbf{v} \in KA\left(\mathbf{D}, \boldsymbol{\chi} \right)$ and all $\boldsymbol{\chi}$ (Appendix).

2.3 In-plane strength domain for running bond masonry

Running bond masonry is made of identical parallelepiped bricks of size b in the horizontal direction 1 (length), a in the vertical direction 2 (height) and t in the third direction (thickness). The building blocks are separated by horizontal continuous bed joints and alternate vertical head joints as shown in Figure 1. e_h is the thickness of the horizontal joints and e_v is the thickness of the vertical joints. Let also Y be the chosen unit cell (Figure 2), G^J the strength domain of the joints, G^{Br} the strength domain of the bricks and π^J, π^{Br} the support functions of G^J and G^{Br} respectively. The aforementioned strength domains are considered known and they are assumed to be convex.

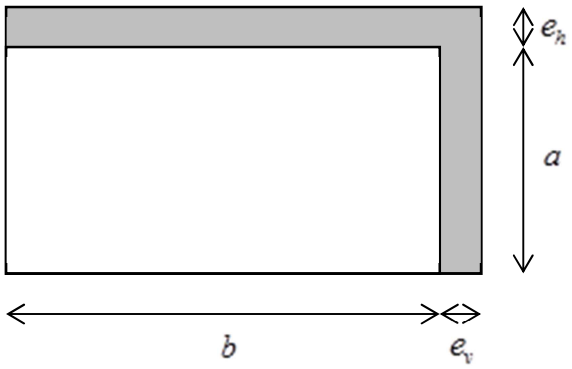

Figure 2. The unit cell.

The idealization of the masonry mortar joints of finite thickness e (e_h, e_v) into two-dimensional interfaces of zero thickness is common in the modeling of masonry structures. In the frame of linear elasticity, Cecchi and Sab (2002) have demonstrated the validity of the aforementioned idealization through asymptotic homogenization. Regarding plasticity, Sahlaoui, Sab, & Heck (2011) have shown that an upper bound of π^{Σ} is asymptotically obtained as the thickness of the joints tends to zero ($e \to 0$, 2D interface):

$$\pi^{\Sigma}(\mathbf{D}) \le \inf_{\mathbf{v}\in KA^*(\mathbf{D},0)} \left\{ \left\langle \pi^{Br}\left(\nabla \otimes^s \mathbf{v}\right)\right\rangle_{Y^*} + \frac{1}{\left|Y^*\right|}\int_{\omega^J} \pi^J\left(\mathbf{n}\otimes^s [\![\mathbf{v}]\!]\right) d\omega^J \right\} \tag{8}$$

where KA^* is the set of kinematically admissible velocity fields (Eq.(3)) of the unit cell Y^* that is obtained from Y as $e_h, e_v \to 0$, $\mathbf{n}$ is the normal to the middle surface ω^J of the joints and $[\![\mathbf{v}]\!] = [\![\mathbf{u}^{per}]\!]$ is the jump of the velocity fields $\mathbf{v}$ and $\mathbf{u}^{per}$ in Eq.(3) across the middle surface ω^J in the direction $\mathbf{n}$ (Figure 3). The second term in the right hand side of the above equation, Eq.(8), expresses the dissipation of the corresponding 2D interface model for the joints. Using standard duality techniques, the interface yield strength domain g^J is the convex domain of the three-dimensional space of the stress vector $\mathbf{t} = \boldsymbol{\sigma}\cdot\mathbf{n}$ defined by:

$$\mathbf{t} \in g^J \Leftrightarrow \mathbf{t}\cdot\mathbf{u} \le \pi^J\left(\mathbf{n}\otimes^s \mathbf{u}\right),\ \forall \mathbf{u} \tag{9}$$

In the following paragraphs we will consider the case of infinitely thin joints ($e_h, e_v \to 0$) and we will use Eq.(8) to propose upped bounds for π^{Σ} in closed form.

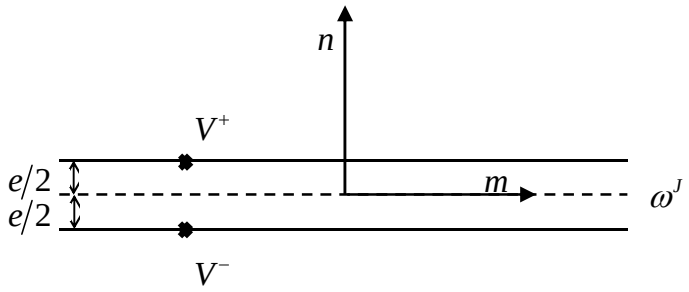

Figure 3. Representation of a plane joint and velocity jump $[\![V]\!] = V^+ - V^-$.

2.4 Upper bound of the strength domain for infinitely resistant building blocks

A first upper bound is obtained by restricting the minimization in Eq.(8) to rigid body motion of the building blocks. This means that the analysis is restricted to those velocity fields in $KA^*(\mathbf{D},\mathbf{0})$ of Y^*, which are piecewise rigid on each block with possible jumps

(discontinuities) at the interfaces. It has been shown by Cecchi and Sab (2002) that the jump of these velocity fields at the interfaces depends only on $\mathbf{D}$ and on one single undetermined rotation Ω. According to the above rigid-body kinematics and velocity jumps, Eq.(8) holds:

$$\pi^{\Sigma}(\mathbf{D}) \le \pi^{\infty}(\mathbf{D}) \equiv \inf_{\Omega} \left\{ \frac{1}{|Y^*|} \int_{\omega^J} \pi^J \left(\mathbf{n} \otimes^s [\![\mathbf{v}]\!] \right) d\omega^J \right\} \tag{10}$$

where π^{∞} is the support function of the in-plane domain G^{∞} of a running bond masonry configuration consisting of infinitely resistant bricks interacting at their interfaces. Hence, $G^{\Sigma} \subset G^{\infty}$.

2.5 Upper bound of the strength domain for blocks of finite strength

Let G^b be the in-plane stress strength domain of the bricks. G^b is the convex set of in-plane stress tensors $(\sigma_{\alpha\beta})$ such that the 3D second order stress tensor $\boldsymbol{\sigma}$ with $\boldsymbol{\sigma} \cdot \mathbf{e}_3 = 0$ is in G^{Br}. Its support function $\pi^b\left((d_{\alpha\beta})\right)$ is obtained by taking the infimum of π^{Br} over all possible 3D second order strain rate tensors having the same in-plane components $(d_{\alpha\beta})$:

$$\pi^b\left((d_{\alpha\beta})\right) = \inf_{d_{13}, d_{23}, d_{33}} \left\{ \pi^{Br}\left(d_{ij}\right) \right\} \tag{11}$$

Using in Eq.(8) the continuous velocity field $\mathbf{v} \in KA^*(\mathbf{D}, \mathbf{0})$ with $u_1^{per}(\mathbf{y}) = c_1 y_3$, $u_2^{per}(\mathbf{y}) = c_2 y_3$ and $u_3^{per}(\mathbf{y}) = c_3 y_3$ leads to the following homogeneous strain rate in the unit cell Y^*:

$$\nabla \otimes^s \mathbf{v} = \begin{pmatrix} D_{11} & D_{12} & \frac{c_1}{2} \\ D_{12} & D_{22} & \frac{c_2}{2} \\ \frac{c_1}{2} & \frac{c_2}{2} & c_3 \end{pmatrix} \tag{12}$$

Here, c_1, c_2 and c_3 are arbitrary real numbers. Taking the minimum of the right-hand side of Eq.(8) over all c_1, c_2, c_3 gives:

$$\pi^{\Sigma}(\mathbf{D}) \leq \pi^{b}(\mathbf{D}) \tag{13}$$

Hence $G^{\Sigma} \subset G^{b}$ and

$$G^{\Sigma} \subset \left(G^{\infty} \bigcap G^{b}\right) \equiv G^{+} \tag{14}$$

The above equation gives an upper bound for the overall strength domain of a running bond masonry wall independently of the materials chosen for the joints and the bricks. Its performance will be investigated in the next paragraphs by means of numerical homogenization and experimental evidence.

3 Finite Element validation of the in-plane strength domain

This section focuses on the validation of the overall strength domain of masonry, which was derived in the above section based on a kinematic approach (Eq.(14)). The validation is performed by comparing the derived strength domain with the exact domain determined by numerical homogenization (Eqs.(5)). For this purpose, the materials for the bricks and the joints have to be specified.

Bricks and mortar are geomaterials, which are commonly described by Coulomb failure criterion. Nevertheless, the numerical treatment of Coulomb yield surfaces can provoke numerical problems related to the non-smoothness of this criterion. Therefore, for the numerical analyses performed in this section the bricks and the joints are considered to obey to a Drucker-Prager criterion. An alternative to Drucker-Prager criterion could be the Lade-Duncan or the Matsuoka-Nakai yield criteria, but their mathematical expression is more complex than the mathematical expression of a Drucker-Prager yield surface.

3.1 Analytical expression of the overall strength domain for Druger-Prager materials

The Drucker-Prager failure criterion has the following form:

$$\boldsymbol{\sigma} \in G \Leftrightarrow f(\boldsymbol{\sigma}) \leq 0 \text{ with } f(\boldsymbol{\sigma}) = q + p\beta - k \tag{15}$$

where $p = \frac{1}{3} tr(\boldsymbol{\sigma})$ is the hydrostatic stress, $\mathbf{s} = \boldsymbol{\sigma} - p\mathbf{I}$ is the deviatoric stress, $q = \sqrt{\frac{3}{2}\mathbf{s}:\mathbf{s}}$, and β, k the Drucker-Prager parameters. We distinguish $(k, \beta) = (k^J, \beta^J)$ for the joints and $(k, \beta) = (k^B, \beta^B)$ for the bricks.

According to Salençon (1983), in the case of interfaces (Figure 3), the Drucker-Prager π-function coincides with the Coulomb support function if:

$$\beta^J = \frac{3\sin\varphi^J}{\sqrt{3 + \sin^2\varphi^J}} \text{ and } k^J = \frac{c^J \beta^J}{\tan\varphi^J} \tag{16}$$

φ^J is the Coulomb friction angle and c^J is the Coulomb cohesion for the joints. In this case, the support function becomes:

$$\pi(\mathbf{n} \otimes^s [\![\mathbf{v}]\!]) = \begin{cases} \dfrac{c^J}{\tan\varphi^J} [\![\mathbf{v}]\!] \cdot \mathbf{n} & \text{if } [\![\mathbf{v}]\!] \cdot \mathbf{n} \geq \|[\![\mathbf{v}]\!]\| \sin\varphi^J \\ +\infty & \text{otherwise} \end{cases} \tag{17}$$

where $[\![\mathbf{v}]\!]$ is the velocity jump across the joint interface ω^J .

According to de Buhan and de Felice (1997) and Sab (2003) for Coulomb interfaces the analytical expression of the strength domain G^∞ is:

$$\boldsymbol{\Sigma} \in G^\infty \Leftrightarrow \begin{cases} \left|\Sigma_{12}^*\right| + \tan\varphi^J \, \Sigma_{22}^* \leq 0 \\ \left(1 + m\tan\varphi^J\right)\left|\Sigma_{12}^*\right| + m\Sigma_{11}^* + \tan\varphi^J \, \Sigma_{22}^* \leq 0 \\ \left(m + \tan\varphi^J\right)\left|\Sigma_{12}^*\right| + m\tan\varphi^J \, \Sigma_{11}^* + \Sigma_{22}^* \leq 0, \quad \text{if } m\tan\varphi^J > 1 \end{cases} \tag{18}$$

where $m = \frac{2a}{b}$ and $\Sigma^*_{\alpha\beta} = \Sigma_{\alpha\beta} - \frac{c^J}{\tan\varphi^J}\delta_{\alpha\beta}$.

The strength domain of the building blocks, G^b, is obtained by setting $\sigma_{13} = \sigma_{23} = \sigma_{33} = 0$ in Eq.(15). Hence, an upper bound G^+ of the system (Eq.(14)) can be analytically determined by adding the following criterion to Eqs.(18):

$$\sqrt{\Sigma_1^2 + \Sigma_2^2 - \Sigma_1\Sigma_2} + \beta^B \frac{\Sigma_1 + \Sigma_2}{3} - k^B \leq 0 \tag{19}$$

where Σ_1, Σ_2 are the principal stresses which are expressed in terms of the stress tensor components as follows:

$$\begin{aligned} \Sigma_1 &= \frac{\Sigma_{11} + \Sigma_{22} + \sqrt{\left(\Sigma_{11} - \Sigma_{22}\right)^2 + 4\Sigma_{12}^2}}{2} \\ \Sigma_2 &= \frac{\Sigma_{11} + \Sigma_{22} - \sqrt{\left(\Sigma_{11} - \Sigma_{22}\right)^2 + 4\Sigma_{12}^2}}{2} \end{aligned} \tag{20}$$

3.2 Numerical homogenization

The in-plane stress may be expressed as follows (biaxial conditions):

$$\boldsymbol{\Sigma} = \Sigma \begin{pmatrix} \cos 2\theta - \xi & -\sin 2\theta \\ -\sin 2\theta & -\cos 2\theta - \xi \end{pmatrix}, \quad \Sigma > 0 \tag{21}$$

or

$$\boldsymbol{\Sigma} = \Sigma \begin{pmatrix} 1 - \chi\cos 2\theta & \chi\sin 2\theta \\ \chi\sin 2\theta & 1 + \chi\cos 2\theta \end{pmatrix} \tag{22}$$

The first case, Eq.(21), corresponds to the state of stress depicted in Figure 4a, while the second, Eq.(22), corresponds to that of Figure 4b. ξ and χ are non-dimensional real parameters varying between -1 and +1 and θ is the angle of the principal axis with respect to the bed joints direction (direction 1) as shown in Figure 4. Therefore, all biaxial states can be

reproduced, i.e. tension/compression (Eq.(21) for $\Sigma > 0$), compression/compression (Eq. (22) for $\Sigma < 0$) and tension/tension (Eq.(22) for $\Sigma > 0$).

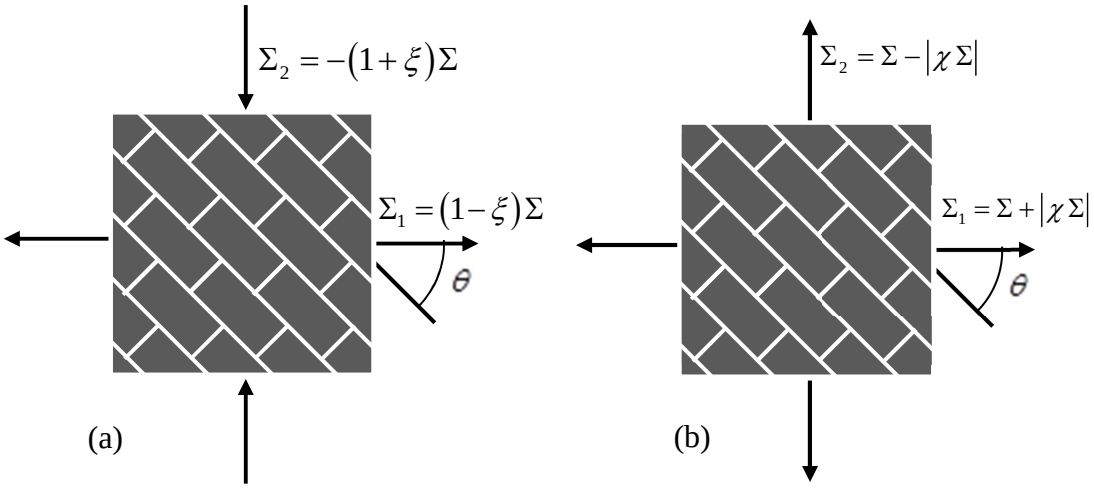

Figure 4. In plane stresses representing, on the left, tension/compression ($\Sigma > 0$) and on the right compression/compression ($\Sigma < 0$) or tension/tension ($\Sigma > 0$).

By means of a Finite Element (FE) software, the maximum value of $\Sigma = \Sigma^{max}$ in Eqs.(21) and (22), such that $\boldsymbol{\Sigma} \in G^{\Sigma}$, can be determined for certain values of θ and ξ or χ. In the frame of perfect associate elasto-plasticity, failure will occur when $\Sigma = \Sigma^{max}$. Herein, the elasto-plastic three-dimensional problem of the unit cell depicted in Figure 1, was solved using the commercial Finite Element code ABAQUS and Σ^{max} was determined for Drucker-Prager materials according to the fitting parameters given in Eq.(16). In Table 1 we present the parameters used for the analyses. The blocks were solid (no holes) and their size was $a = 38mm$, $b = 115mm$ and $t = 55mm$. The effect of the joints' thickness was investigated by varying (e_h, e_v). Both the blocks and the joints were modeled with three dimensional solid elements.

Table 1. Mechanical parameters for the bricks and the mortar used for the comparison of the numerical and analytical homogenization schemes.

Bricks	
Coulomb cohesion, c^b	4.3 MPa
Coulomb friction angle, φ^b	30°
Elastic modulus	6740 MPa
Poisson ratio	0.17
Mortar	
Coulomb cohesion, c^J	0.35 MPa
Coulomb friction angle, φ^J	40°
Elastic modulus	1700 MPa
Poisson ratio	0.05

It is worth mentioning that the selected Young's moduli were only used for the numerical homogenization scheme presented in this section, which is performed in order to validate the analytical strength domain derived through Eq.(14). In the frame of perfect associate elastoplasticty the analytical and numerical homogenization schemes should provide the same ultimate strength independently of the chosen elastic moduli. Different approaches (e.g. damage mechanics) may show a dependence on the elastic moduli and may provide more accurate results (provided that the necessary mechanical parameters can be adequately calibrated based on experimental tests) but the advantage of the present approach is that it leads to an analytical expression of the strength domain based on a solid theoretical framework.

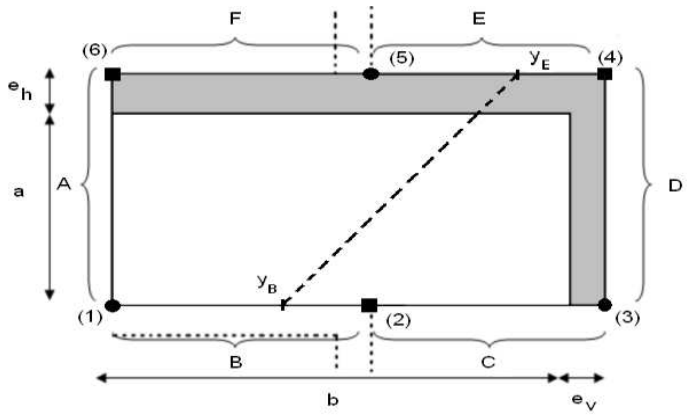

Figure 5. Section of the unit cell along the middle plane of the masonry and notation of its interactions with the adjacent cells (see also Figure 1).

Periodic boundary conditions were imposed at the unit cell. Therefore, the nodal degrees of freedom at opposite faces were paired. In Figure 5, A, B, C, D, E, F denote the six faces of the boundary of the unit cell. Notice that the infinite microstructure, i.e. the geometry of the elementary cell, remains invariant to translations by vectors joining node (5) with node (1) or (3) and vectors joining node (4) with node (6) or (2). Consequently, face E should be matched by periodicity conditions with face B, face D should by matched with face A and face F with face C. Hence, the periodic conditions at the unit cell are:

$$\mathbf{v}(y_E)-\mathbf{v}(y_B)=\mathbf{D}\cdot(y_E-y_B)=\begin{pmatrix}\frac{b+e_v}{2}D_{11}+(a+e_h)D_{12}\\ \frac{b+e_v}{2}D_{12}+(a+e_h)D_{22}\\ 0\end{pmatrix}$$

$$\mathbf{v}(y_D)-\mathbf{v}(y_A)=\mathbf{D}\cdot(y_D-y_A)=\begin{pmatrix}(b+e_v)D_{11}\\ (b+e_v)D_{12}\\ 0\end{pmatrix} \tag{23}$$

$$\mathbf{v}(y_F)-\mathbf{v}(y_C)=\mathbf{D}\cdot(y_F-y_C)=\begin{pmatrix}-\frac{b+e_v}{2}D_{11}+(a+e_h)D_{12}\\ -\frac{b+e_v}{2}D_{12}+(a+e_h)D_{22}\\ 0\end{pmatrix}$$

where $\mathbf{v}^{(k)}$ are the degrees of freedom of node $k=1,2,...,6$ as shown in Figure 5. It should be mentioned that as far it concerns the numerical implementation and homogenization in static conditions, there is no need to distinguish between velocities and displacements, and strains from strain rates. Equations (23) may be used to determine the components of $\mathbf{D}$ in terms of the nodal degrees of freedom, $k=1,2,...,6$. Indeed setting the nodal degrees of freedom $\mathbf{v}^{(1)}=0$ we obtain:

$$D_{11}=\frac{v_1^{(3)}}{b+e_v},\quad D_{12}=\frac{v_2^{(3)}}{b+e_v},\quad D_{22}=\frac{v_2^{(5)}-\frac{1}{2}v_2^{(3)}}{a+e_h}, \tag{24}$$

Furthermore, Eqs.(23) may be expressed in terms of the nodal degrees of freedom $\mathbf{v}^{(k)}$ and the periodic boundary conditions may be set node by node in the finite element model of the unit cell. Using Eqs.(24), the kinematic scalar variable, ε, which is conjugate in energy with the stress scalar variable, Σ (Eq.(21)), for tension/compression is given by:

$$\varepsilon=\frac{1}{\Sigma}\boldsymbol{\Sigma}:\mathbf{D}=\frac{\cos 2\theta-\xi}{b+e_v}v_1^{(3)}+\left(\frac{1}{2}\frac{\cos 2\theta+\xi}{a+e_h}-2\frac{\sin 2\theta}{b+e_v}\right)v_2^{(3)}-\frac{\cos 2\theta+\xi}{a+e_h}v_2^{(5)} \tag{25}$$

and for tension/tension or compression/compression by:

$$\varepsilon = \frac{1}{\Sigma}\boldsymbol{\Sigma} : \mathbf{D} = \frac{1-\chi\cos 2\theta}{b+e_v} v_1^{(3)} - \left(\frac{1}{2}\frac{1+\chi\cos 2\theta}{a+e_h} - \frac{2\chi\sin 2\theta}{b+e_v} \right) v_2^{(3)} + \frac{1+\chi\cos 2\theta}{a+e_h} v_2^{(5)} \quad (26)$$

The numerical simulations of the three dimensional unit cell were performed by increasing ε until the ultimate load that corresponds to $\Sigma^{\max}$. In Figure 6 we present an example of the deformation of the three dimensional unit cell that was used in the numerical homogenization scheme. The contours represent the minimum principal stresses in MPa developed in the unit cell for uniaxial compression normal to the bed joints ($\xi = 1$, $\theta = 0$ and $e_h = e_v = 5mm$). Notice the excess deformation of the joints in relation to the deformation of the block. It is worth mentioning that the mortar is in a triaxial stress state and not in plane stress or plane strain conditions. This justifies, the general formulation presented in section 2 and the fact that a three dimensional stress and kinematic field were employed during the homogenization procedure.

The overall stress components $\Sigma_{\alpha\beta} = \langle \sigma_{\alpha\beta} \rangle$ are computed by averaging the stress values at the Gauss points. Figure 7 shows the obtained stress-strain (Σ, ε) curve in the case of uniaxial compression normal to the bed joints of the unit cell, i.e. for $\xi = 1$ and $\theta = 0^\circ$, and for $e_h = e_v = 5mm$. The ultimate stress $\Sigma^{\max}$ is obtained as the asymptotic value of Σ for increasing ε (Figure 7). According to Eq.(21), the ultimate uniaxial compressive strength is equal to $\Sigma_{22} = -2\Sigma^{\max}$. In the next paragraphs we present the results from the various numerical analyses performed in order to validate G^+.

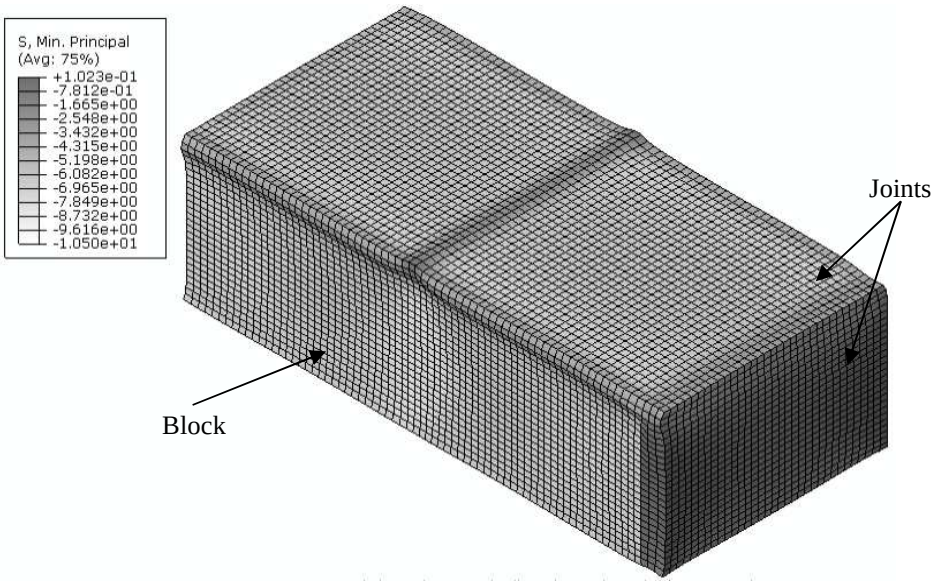

Figure 6. Example of the deformation of the three dimensional unit cell that was used in the numerical homogenization scheme. The contours represent the minimum principal stresses (in MPa) developed at the unit cell for uniaxial compression normal to the bed joints ($\xi = 1$, $\theta = 0$ and $e_h = e_v = 5mm$). Notice the excess deformation of the mortar at the joints in relation to the deformation of the block. The mortar is in a triaxial stress state.

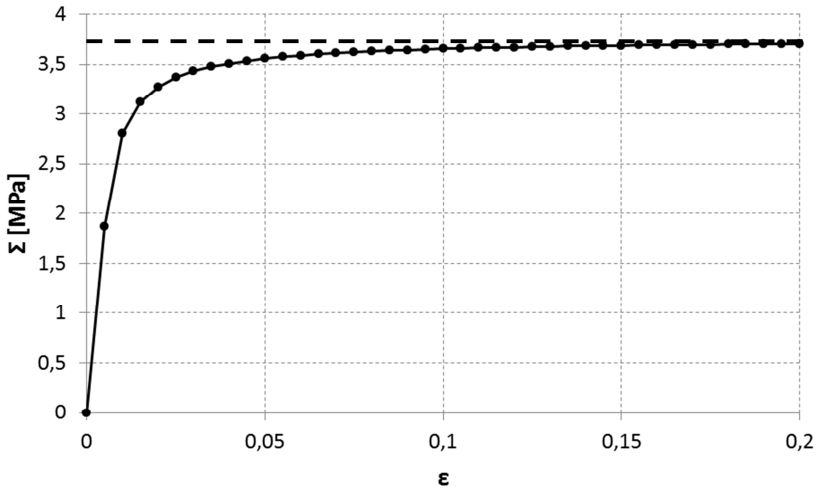

Figure 7. Example of a stress-strain (Σ, ε) curve derived through numerical homogenization of the unit cell for vertical compression ($\xi = 1$, $\theta = 0$ and $e_h = e_v = 5mm$). The ultimate stress

Σ^{max} is obtained as the asymptotic value of Σ for increasing ε (dotted line). The uniaxial compression strength of the masonry is then $\Sigma_{22} = -2\Sigma^{max}$ (see Eq.(21))

3.3 Comparison of the analytical and numerical in-plane strength domains

The in-plane strength domain that was derived analytically in the previous paragraphs (G^{+}) consists an upper bound of the strength domain of the masonry structure (G^{Σ}). Therefore, a comparison of the analytical result with the strength domain that was calculated by means of numerical homogenization (G^{Num}) is presented in this paragraph.

Several numerical simulations were performed on the elementary cell for different angles θ and loading combinations (Σ_1, Σ_2). In particular, the following biaxial configurations were investigated: $\xi = 1.0$ (uniaxial compression normal to the bed joints $\Sigma_1 = 0$, $\Sigma_2 = -2\Sigma$), $\xi = 0.8$, $\xi = 0.5$, $\xi = 0.0$, $\xi = -0.5$ and $\xi = -1.0$ (uniaxial tension normal to the head joints $\Sigma_1 = 2\Sigma$, $\Sigma_2 = 0$). Moreover, three different joint thicknesses were considered, i.e. $e_h = e_v = 0.1mm$, $e_h = e_v = 2.0mm$ and $e_h = e_v = 5.0mm$ corresponding respectively to the 0.3%, 5.3% and 13.2% of the height of the block.

In Figure 8 to Figure 13 the numerical (G^{Num}) and the analytical (G^{+}) strength domains are juxtaposed for the three different joint thicknesses. It is worth mentioning that all the analytical calculations in the present paper have been performed with the symbolic language mathematical package Wolfram Mathematica. The numerical strength domain is traced for different values of the angle θ. As it was previously described the overall analytical strength domain G^{+} is the intersection of three domains. These are the strength domain of the blocks G^{b} (Eq.(15)) and the strength domains of the bed (Eq.(18)a&b) and head (Eq.(18)c&d) joints (G^{∞}). In Figure 10 the aforementioned strength domains are clearly distinguished. If the

failure of the blocks was not taken into account the strength domain of the masonry would be unbounded, which is unrealistic. The numerically calculated ultimate stresses coincide with the analytical yield surfaces that correspond to the failure of the joints in all the biaxial configurations tested (Figure 4). For instance, in Figure 11 we observe that for $10^{\circ} \le \theta \le 90^{\circ}$ the ultimate strength falls exactly at the boundary of the analytical strength domain. However, this is not the case when the failure of the unit cell is attributed to a combination of the failure of blocks and of the failure of the joints (e.g. Figure 8 for $0^{\circ} \le \theta \le 40^{\circ}$ and $\theta = 90^{\circ}$, Figure 11 for $\theta = 0^{\circ}$ etc.). In this case the thickness of the joints plays a crucial role and the ultimate stresses derived by numerical homogenization fall inside the analytical yield surface.

This is not an astonishing result as the analytical strength domain is an upper bound of the exact strength domain of the system. This discrepancy is stressed also by Milani et al. (2006b). In Figure 14 we present the ratio of the ultimate strength that was calculated by numerical homogenization (Σ^{Num}) over the upper bound of its value that was derived analytically by the limit analysis theory (Σ^{+}) in function of the joints' thickness, $e = e_h = e_v$ for various values of ξ and for $\theta = 0°$. Similar results are also obtained for the biaxial states described in Figure 4b as it is shown in Figure 15.

Generally, the thinner the joints are, the better is the convergence of the numerical results to the analytical yield surface. This behavior can be qualitatively explained by comparing the plastic deformations of the different analyses performed with different joint thicknesses. In particular, at Figure 16 and Figure 17 we present the magnitude of the plastic deformations for $\xi = 1$, $\theta = 30^{\circ}$ and, respectively, for $e = 0.1mm$ and $e = 5.0mm$. According to the numerical results (see Figure 8 and Figure 14) the analytical strength domain approximates quite well the numerical one for $e = 0.1mm$, while there is an error of approximate 20% for the case of $e = 5.0mm$ (13.2% of the height of the block). Focusing on Figure 16 we observe

that the resulting plastic deformations at the block are almost homogeneous and therefore the assumed homogeneous deformation in the unit cell for the analytical determination of the yield surface (Eq.(12)) is consistent. However, this is not the case for the thicker joints, where the plastic deformations are clearly not homogeneous (Figure 17) and consequently the considered kinematic admissible field that was introduced through Eq.(12) is not representative.

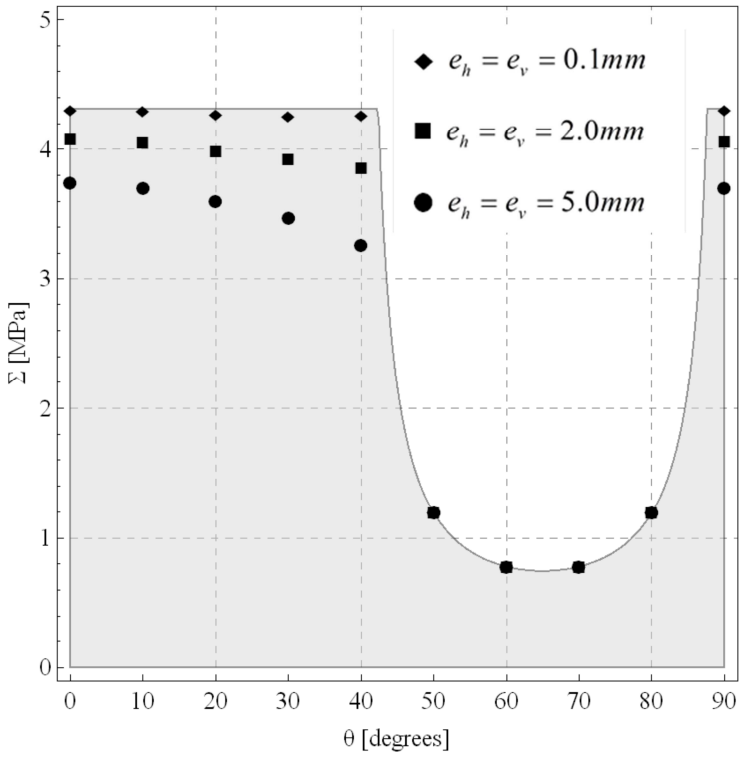

Figure 8. Comparison of the strength domains for uniaxial compression ($\xi = 1$) and for various angles θ. The shaded region represents the analytical strength domain (G^+) and the markers the ultimate strength of the unit cell that was derived by numerical homogenization. For thin joints the numerical results approach the analytically derived upper bound G^+. For $\theta = 0°$ the uniaxial compression strength of the masonry is found by multiplying Σ^{max} by a factor of two (see Eq.(21)).

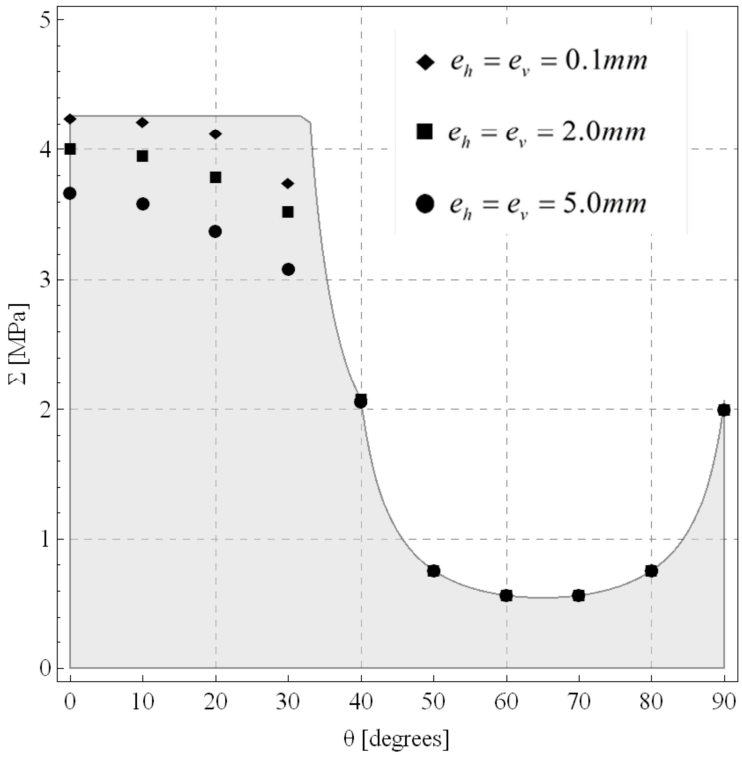

Figure 9. Comparison of the strength domains for $\xi = 0.8$ and for various angles θ. The shaded region represents the analytical strength domain (G^+) and the markers the ultimate strength of the unit cell that was derived by numerical homogenization. For thin joints the numerical results approach the analytically derived upper bound G^+.

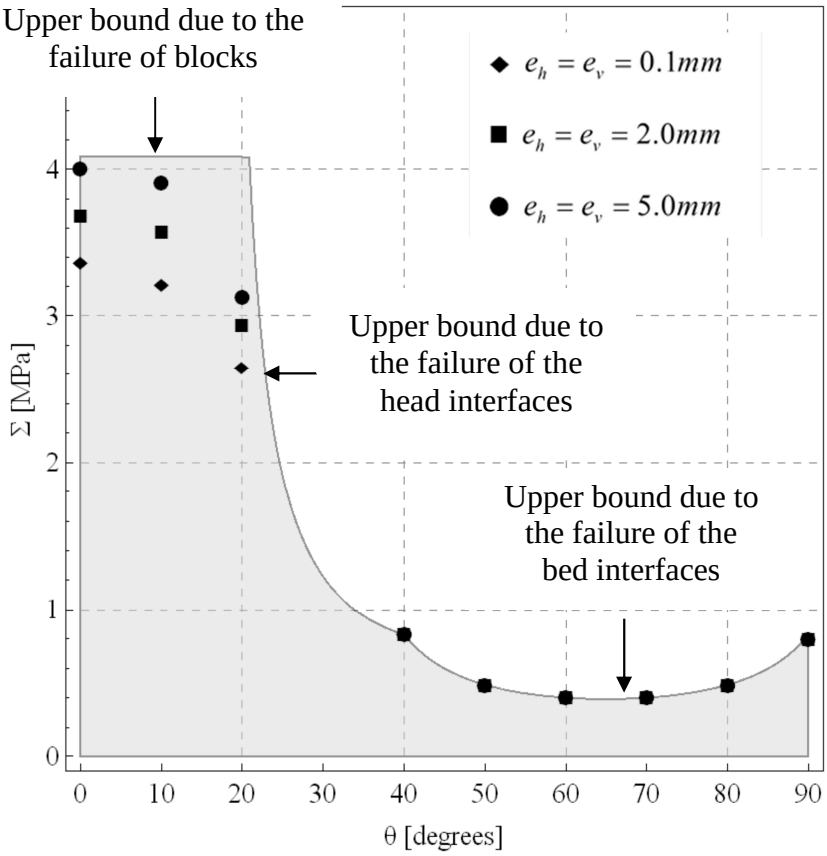

Figure 10. Comparison of the strength domains for $\xi = 0.5$ and for various angles θ. The shaded region represents the analytical strength domain (G^+) and the markers the ultimate strength of the unit cell that was derived by numerical homogenization. For thin joints the numerical results approach the analytically derived upper bound G^+.

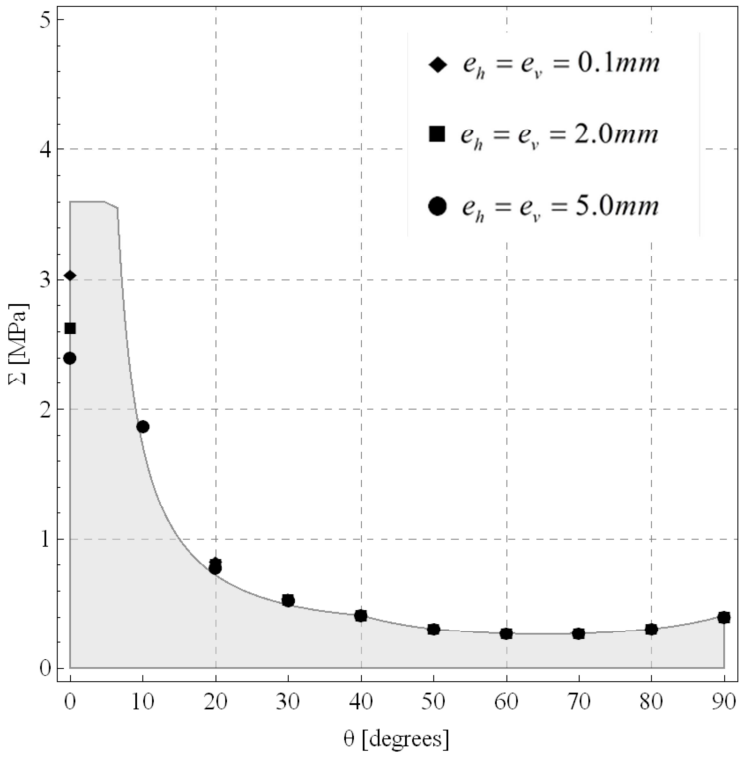

Figure 11. Comparison of the strength domains for $\xi = 0.0$ and for various angles θ. The shaded region represents the analytical strength domain (G^+) and the markers the ultimate strength of the unit cell that was derived by numerical homogenization.

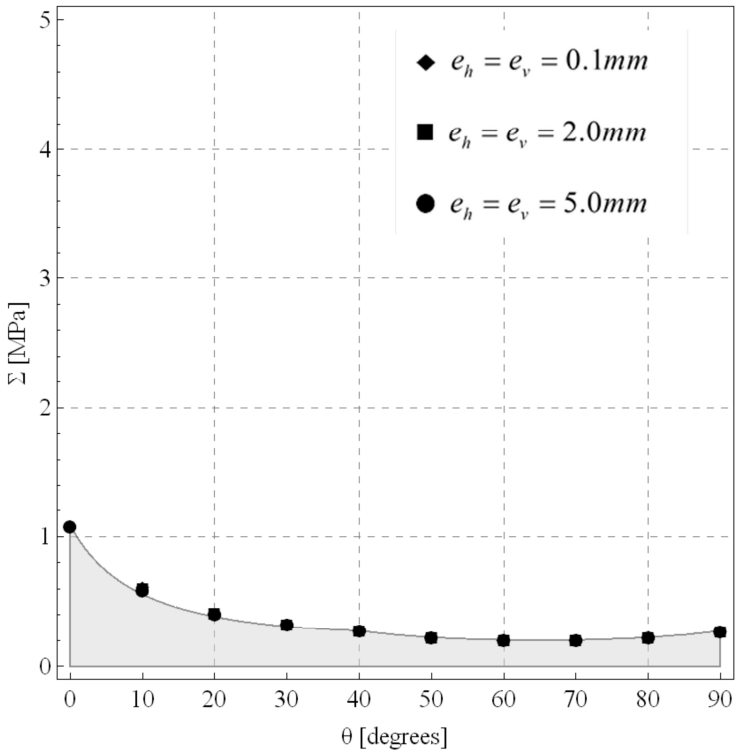

Figure 12. Comparison of the strength domains for $\xi = -0.5$ and for various angles θ. The shaded region represents the analytical strength domain (G^+) and the markers the ultimate strength of the unit cell that was derived by numerical homogenization.

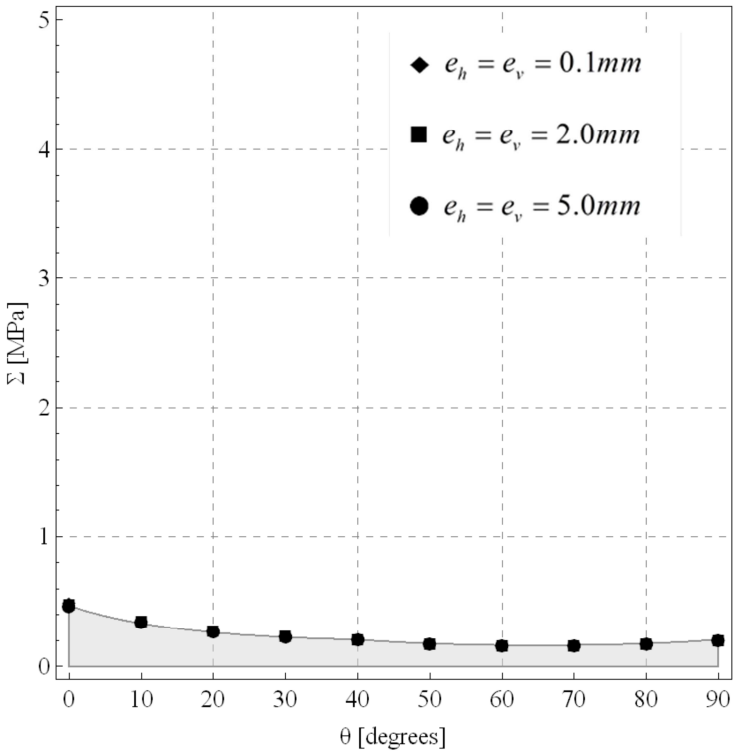

Figure 13. Comparison of the strength domains for uniaxial tension ($\xi = -1$) and for various angles θ. The shaded region represents the analytical strength domain (G^+) and the markers the ultimate strength of the unit cell that was derived by numerical homogenization.

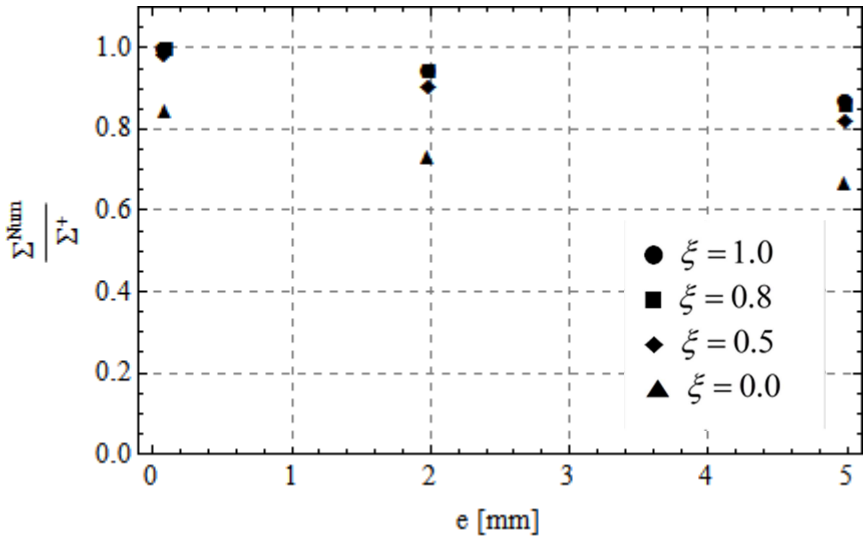

Figure 14. Ratio of the ultimate strength of the unit cell that was calculated by numerical homogenization (Σ^{Num}) over the upper bound of its value that was derived analytically by the theory of limit analysis (Σ^{+}) in function of the joints' thickness, $e = e_h = e_v$ for various values of ξ and for $\theta = 0°$. For thin joints the numerical results approach the analytically derived upper bound G^{+}.

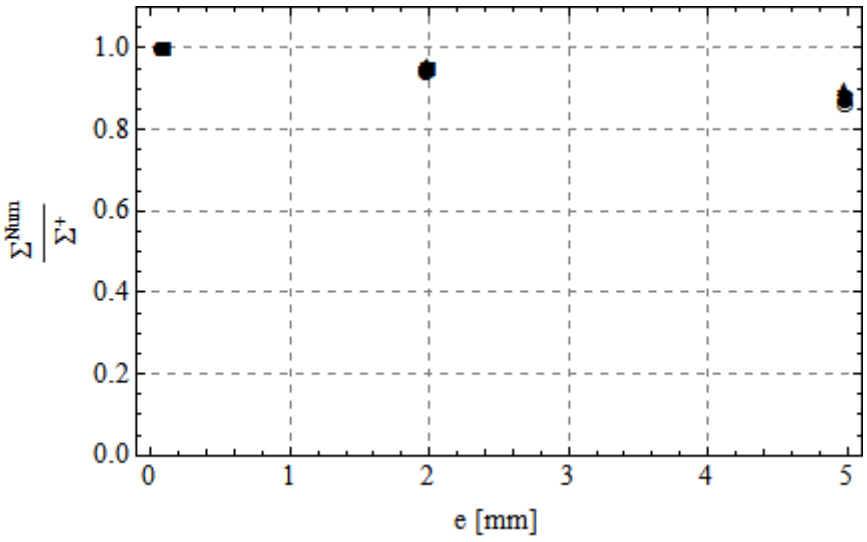

Figure 15. Ratio of the ultimate strength of the unit cell that was calculated by numerical homogenization (Σ^{Num}) over the upper bound of its value that was derived analytically by the theory of limit analysis (Σ^{+}) in function of the joints' thickness, $e = e_h = e_v$ for various values of χ and for $\theta = 0°$. The influence of χ is quite limited. For thin joints the numerical results converge to the analytically derived upper bound G^{+}.

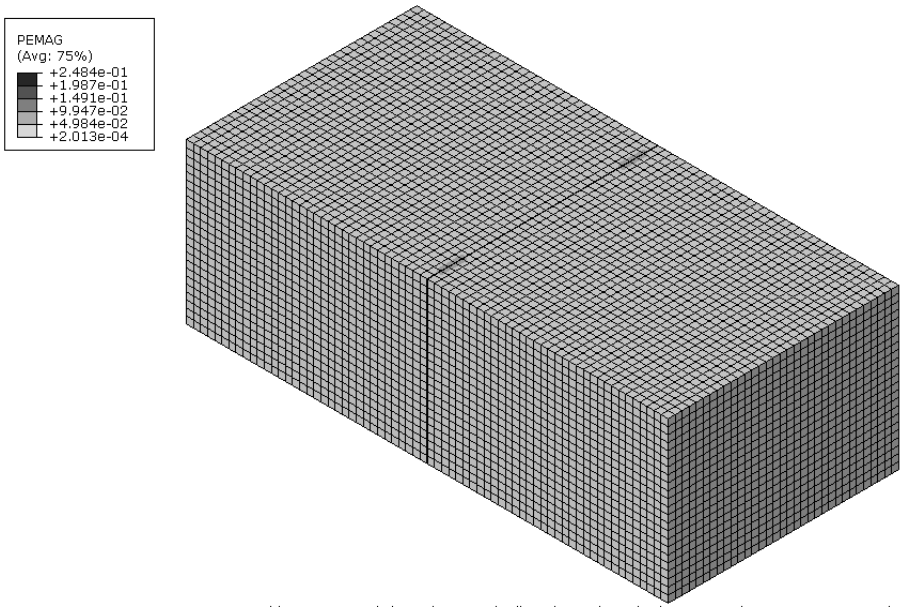

Figure 16. Contours of the magnitude of the plastic deformations developed inside the masonry unit (joints are not shown) for $\xi = 1$ and $\theta = 30^{\circ}$. The plastic deformations are homogeneous except in the middle of the block where the deformation is localized.

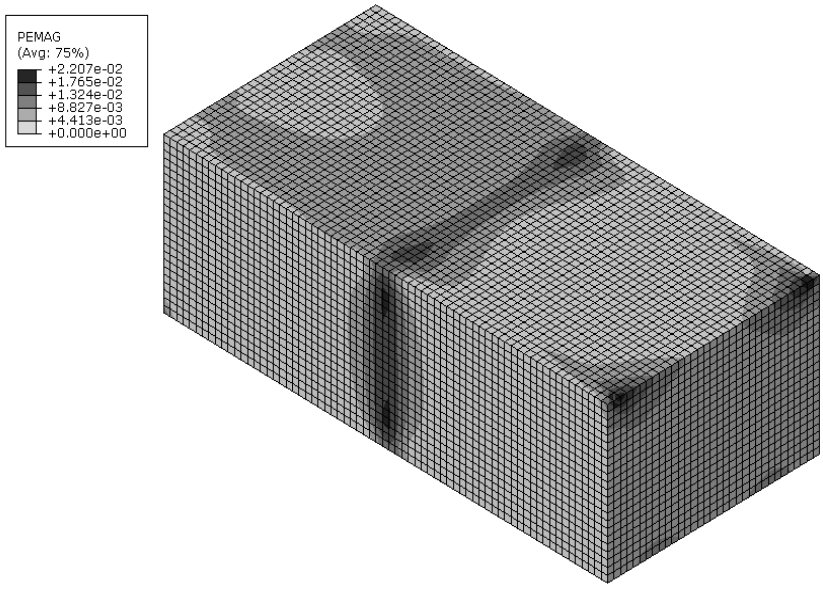

Figure 17. Contours of the magnitude of the plastic deformations developed inside the masonry unit (joints are not shown) for $\xi = 1$ and $\theta = 30^{\circ}$. The plastic deformations are not homogeneous and they are more important in the middle of the unit due to the head joints.

4 Comparison with experimental results

The effect of the thickness of the joints and the difference of the analytically derived strength domain with the numerical one was quantified and justified in the previous section. The analytical model overestimates the strength of the masonry in some biaxial load cases. This difference is of the order of 20% for the thicker joints (Figure 14, Figure 15). Moreover, the non-homogeneous stress field inside the masonry units that was discussed in the previous section leads to the development of tensile stresses (cf. Figure 16 and Figure 17). Consequently, the analytical model might also overestimate the resistance of the masonry due to the fact that it does not take into account the brittle behavior of the bricks in tension and the related crack formation. In particular, experiments performed by Sahlaoui et al. (2011) on non-uniformly loaded masonry units (Figure 18) showed that the ultimate compressive load is on the average 60% lower than the ultimate compressive load of the same units under uniform loading. This is a well-known issue in masonry structures and a similar drop of the compressive strength was also noticed by Page (1981, 1983). According to Page, the mean compressive strength of four-high stack bonded piers was 65% the compressive strength of half-scaled bricks. In particular the mean compressive strength of the half-scale bricks was 15.41 MPa (coefficient of variation of 18%) while the mean compressive strength of the four-high stack bonded piers was only 9.85 MPa (coefficient of variation of 9%).

Finally, due to scale effects that are inherent to geomaterials and due to experimental difficulties related to the influence of the friction between the specimen and the plates of the loading frame (Brencich, Corradi, & Gambarotta, 2008; Kourkoulis & Ganniari-Papageorgiou, 2010) the determination of the compressive strength and generally the assessment of the mechanical characteristics of the masonry based on the strength of its units

is not a trivial issue. Therefore, the determination of the overall strength of masonry based on the individual strength of its constituents is, experimentally, not an easy task.

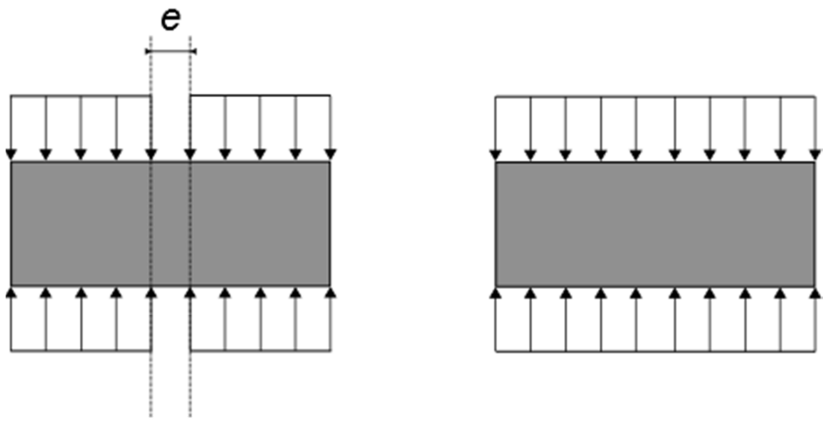

Figure 18. Schematic representation of tests performed on non-uniformly loaded bricks (left) and on uniformly loaded masonry units (right). Because of the vertical (head) joints of thickness *e*, the stress field developed inside the bricks is not uniform leading to tensile stresses and crack formation.

In the early 1980s, Page published the results of a series of experimental tests of masonry panels subjected to in-plane biaxial monotonic loading. Here we use these results in order to assess the validity of the proposed analytically derived strength domain. A classical Coulomb yield surface is considered for the masonry units. For the reasons presented above (brittle behavior, effect of joint thickness, scale effects, experimental difficulties) the in-situ compressive strength of the bricks will be taken equal to the resistance of the four-high stack bonded piers tested by Page (1981, 1983), i.e. equal to 10 MPa. Moreover, in order to account for the failure of the mortar and the mortar-brick debonding and similar to Page (1978), a bilinear Coulomb criterion is considered herein for the interfaces (Figure 19).

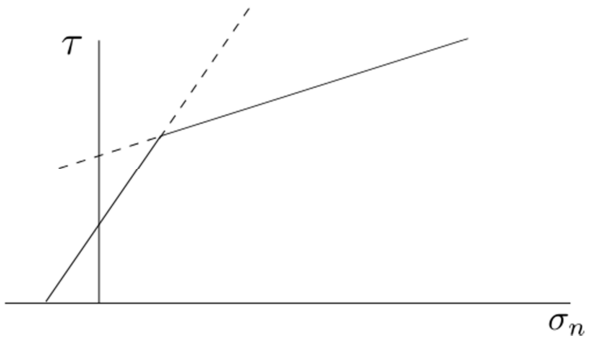

Figure 19. Schematic representation of a bilinear Coulomb criterion for the interfaces (solid lines). τ is the shear stress and σ_n is the normal stress at the interface.

It follows from Eq.(10) that the same relations as in Eq.(18) hold in the case of interfaces obeying to a bilinear Coulomb criterion. According to Eq.(14) the strength domain of the masonry is expressed in closed form as follows:

$$\begin{cases} \left|\Sigma_{12}\right| + \tan\varphi_\gamma^J \,\Sigma_{22} - c_\gamma^J \le 0 \\ \left(1 + m\tan\varphi_\gamma^J\right)\left|\Sigma_{12}\right| + m\Sigma_{11} + \tan\varphi_\gamma^J \,\Sigma_{22} - c_\gamma^J\left(\dfrac{m}{\tan\varphi_\gamma^J} + 1\right) \le 0, \quad \text{if } m\tan\varphi_\gamma^J \le 1 \\ \left(m + \tan\varphi_\gamma^J\right)\left|\Sigma_{12}\right| + m\tan\varphi_\gamma^J \,\Sigma_{11} + \Sigma_{22} - c_\gamma^J\left(\dfrac{1}{\tan\varphi_\gamma^J} + m\right) \le 0, \quad \text{if } m\tan\varphi_\gamma^J > 1 \\ \left|\Sigma_1 - \Sigma_2\right| + \left(\Sigma_1 + \Sigma_2\right)\sin\varphi^B - 2c^B\cos\varphi^B \le 0 \end{cases} \tag{27}$$

where $\gamma = 1$ or 2 . The mechanical parameters of the masonry constituents are given in Table 2. It is worth emphasizing that the values for the dimensions and for the mechanical properties of the bricks and the joints could not be extracted from the articles of Page. Similar values as in Milani et al. (2006b) were taken into account for the dimensions and for the compressive to tensional strength ratio of the bricks. In particular the dimensions of the bricks were 110x50x35 mm^3 ($m = \dfrac{2a}{b} = 0.9$) and the compressive to tensional strength ratio was considered equal to 6.

Table 2. Estimation of the mechanical parameters of the bricks and of the mortar that were used for the comparison of the analytically derived strength domain and the experimental results of Page (1981).

Bricks	
Coulomb cohesion, c^b	2 MPa
Coulomb friction angle, φ^b	45°
Mortar	
Coulomb cohesion, c_1^J	0.35 MPa
Coulomb friction angle, φ_1^J	39°
Coulomb cohesion, c_2^J	2 MPa
Coulomb friction angle, φ_2^J	17°

In Figure 20 to Figure 22 we present the comparison of the analytical strength domain with the experimental results of Page (1981) for various angles θ. A quite good agreement is observed.

The finite strength of the building blocks may be quite important for structural applications. For instance, if we consider the simple example of a masonry panel subjected to vertical compression ($\Sigma_{11}=\Sigma_{12}=0$ and $\Sigma_{22}<0$ (compression), $\Sigma_1=0$ and $\Sigma_2=\Sigma_{22}<0$) Eqs.(27) become:

$$\begin{cases} \Sigma_{22} \le \dfrac{c_\gamma^J}{\tan\varphi_\gamma^J} \\ \Sigma_{22} \le \dfrac{c_\gamma^J}{\tan\varphi_\gamma^J}\left(\dfrac{m}{\tan\varphi_\gamma^J}+1\right), \quad \text{if } m\tan\varphi_\gamma^J \le 1 \\ \Sigma_{22} \le c_\gamma^J\left(\dfrac{1}{\tan\varphi_\gamma^J}+m\right), \quad \text{if } m\tan\varphi_\gamma^J > 1 \\ \Sigma_{22} \ge -\dfrac{2c^B\cos\varphi^B}{1-\sin\varphi^B} \end{cases} \tag{28}$$

The first three inequalities are automatically satisfied for vertical compression ($\Sigma_{22}<0$). In other words the joints do not fail. This is in accordance with building standards which they do

not account the compressive strength of the mortar in the case of thin joints (triaxial state/confinement). On the contrary the resistance of masonry is limited by the resistance of the blocks. The strength domain is not unbounded in compression. In particular the homogenized compression strength is approximately -9.66 MPa. The consideration of the finite resistance of the blocks might play a crucial role in reducing the load bearing capacity of masonry and change the failure mechanism.

The analytically derived strength domain (Eqs.(18), (27) and more generally the domain given in Eqs.(14)) covers any macroscopic in-plane stress state. Therefore, it can be implemented in appropriate Finite Element codes based on multisurface plasticity in order to solve more complicated structural examples. Nevertheless, such examples exceed the scope of the present work, which focuses on the constitutive description of masonry.

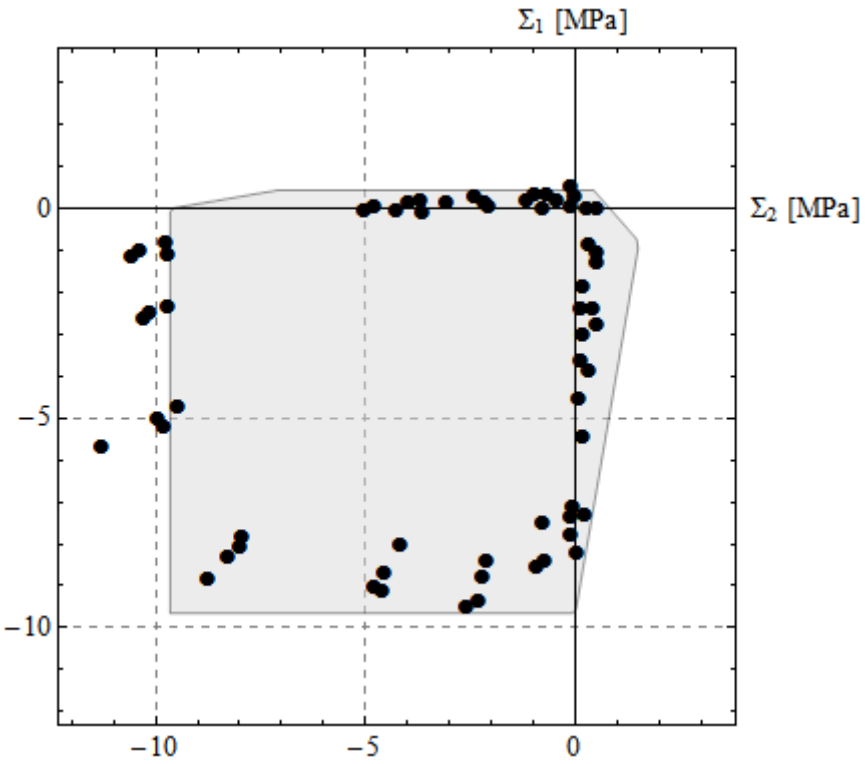

Figure 20. Comparison of the analytical strength domain (shaded region) with the experimental results of Page (1981) for $\theta = 0^\circ$.

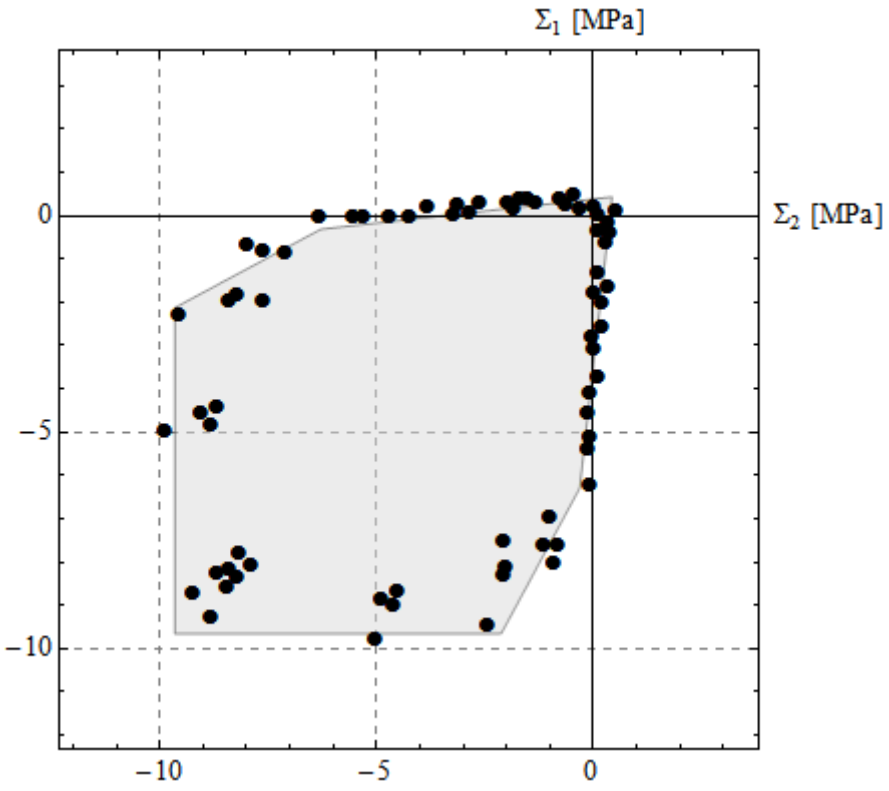

Figure 21. Comparison of the analytical strength domain (shaded region) with the experimental results of Page (1981) for $\theta = 22.5^\circ$.

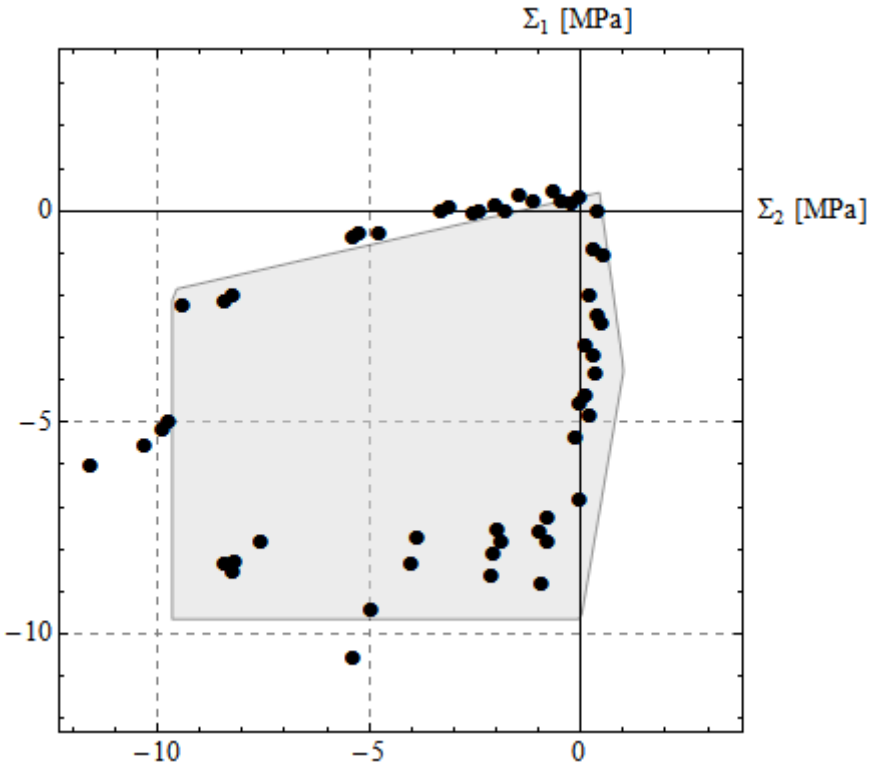

Figure 22. Comparison of the analytical strength domain (shaded region) with the experimental results of Page (1981) for $\theta = 45^{\circ}$.

5 Conclusions

It is well known that the macroscopic mechanical properties of masonry differ from the mechanical properties of its constituents, i.e. of the building blocks (bricks) and of the mortar (if present). Generally, in structural analysis of masonry structures, the determination of the ultimate/limit strength of masonry is a quite important topic. Due to the complexity and the heterogeneity of the material, most of the failure criteria that are generally proposed in the literature are based on macroscopical and phenomenological considerations. In the present paper, a micromechanical model is formulated that takes into account the three-dimensional non-elastic behavior of the microstructure of a periodic masonry wall structure. Based on a rigorous definition of the microstructure and by using basic tools of convex analysis and limit analysis theory, it was made possible to pursue further the results of de Buhan & de Felice

(1997) and derive analytically the overall strength domain of a masonry wall made of building blocks of finite strength and mortar. A kinematic limit analysis approach was followed using a three-dimensional stress and kinematic field. Unlike similar homogenization approaches for masonry (e.g. de Buhan & de Felice, 1997; Milani et al., 2006), no plane stress conditions are a priori assumed in the present work and the problem is treated in three dimensions. The reason is that the stress state in the mortar cannot be precisely described either by plane stress or plane strain conditions.

In order to assess the validity and the efficiency of the derived domain, which is an upper bound of the exact one, a numerical homogenization scheme was used for certain geometrical and mechanical parameters of the unit cell. It was found that the difference between the analytical strength domain and the numerical one is insignificant for masonry structures with thin joints. However, for structures with thicker joints the error increases and the analytical domain overestimates to some extent the ultimate strength. Finally, the derived strength domain was compared to the experimental results of Page and a quite good agreement was observed.

The proposed strength domain is general enough and according to the mechanical resistance of the masonry constituents it can be expressed through simple closed-form inequalities. The dimensions of the units, the frictional behavior of the mortar-brick interfaces and the in-situ mechanical strength of the masonry units have to be characterized in order to define the analytical strength domain of the brickwork. These parameters can be determined from simple experiments of the mortar-brick interface and of the masonry units. Nevertheless, due to the brittle behavior of the bricks, the effect of the joint thickness, the inherent scale effects of geomaterials and the experimental difficulties for obtaining the compressive strength of the bricks, the determination of the in-situ strength of the masonry constituents is not trivial. Experimental tests of single masonry piers in compression seem to be more representative for

characterizing the in-situ compressive strength of the masonry units and can be used for selecting the appropriate parameters.

The proposed strength domain can be used for limit analyses or for finite element simulations of a brickwork (e.g. de Felice et al., 2009). Nevertheless, the application of the present model to masonry structures with comprehensive examples and structural applications exceeds the scope of the present work and it will be presented in a future publication. Finally, existing phenomenological models (e.g. Ottosen, 1977; Syrmakezis & Asteris, 2001) may be calibrated using the derived analytical anisotropic strength domain. In this way numerous and laborious experiments on masonry panels can be avoided.

Appendix

In this appendix we extend the results of Dallot & Sab (2008a, 2008b). Symmetric periodic plates have interesting features which are detailed hereafter. Recall that G^N is the projection of $G_p^{\hom}$ on the subspace $(\mathbf{N},\mathbf{M}=0)$. Similarly,

$$G^M = \left\{\mathbf{M} \mid \exists \mathbf{N}, (\mathbf{N},\mathbf{M}) \in G_p^{\hom}\right\} \tag{A.1}$$

is the projection of $G_p^{\hom}$ on the subspace $(\mathbf{N}=0,\mathbf{M})$ and its corresponding support function is:

$$\pi^M(\boldsymbol{\chi}) = \pi_p^{\hom}(0,\boldsymbol{\chi}) \tag{A.2}$$

The intersection of $G_p^{\hom}$ with the subspace $(\mathbf{N},\mathbf{M}=0)$ is noted:

$$G^{(N,0)} = \left\{\mathbf{N} \mid \exists (\mathbf{N},0) \in G_p^{\hom}\right\} \tag{A.3}$$

Its corresponding support function is:

$$\pi^{(N,0)}(\mathbf{D}) = \inf_{\boldsymbol{\chi}} \pi_p^{\hom}(\mathbf{D},\boldsymbol{\chi}) \tag{A.4}$$

Finally,

$$G^{(0,M)} = \left\{ \mathbf{M} \,|\, \exists (0,\mathbf{M}) \in G_p^{\hom} \right\} \tag{A.5}$$

is the intersection of $G_p^{\hom}$ with the subspace $(\mathbf{N}=0,\mathbf{M})$ and its corresponding support function is:

$$\pi^{(0,M)}(\boldsymbol{\chi}) = \inf_{\mathbf{D}} \pi_p^{\hom}(\mathbf{D},\boldsymbol{\chi}) \tag{A.6}$$

For symmetric periodic plates we have the following property:

$$G^N = G^{(N,0)} \text{ and } G^M = G^{(0,M)} \tag{A.7}$$

Indeed, recall that two closed convex sets are equal if, and only if, their corresponding support functions are identical. It can be seen that $\mathbf{v}$ is in $KA(\mathbf{D},\boldsymbol{\chi})$ if, and only if, its symmetric image $\mathbf{v}^*$ is in $KA(\mathbf{D},-\boldsymbol{\chi})$ where $\mathbf{v}^*$ is given by: $\mathbf{v}^*(\mathbf{y}) = -\mathbf{v}(-\mathbf{y})$ for all $\mathbf{y}$ in Y. Moreover, due to the symmetry condition ($G(\mathbf{y}) = G(-\mathbf{y})\ \forall \mathbf{y} \in Y$), we have $\pi(\mathbf{y}, \nabla \otimes^s \mathbf{v}) = \pi(-\mathbf{y}, \nabla \otimes^s \mathbf{v}^*)$. Using, the kinematic definition of Eq.(3) and the fact that $\pi(\mathbf{y},\cdot)$ is positively homogeneous of degree one, we easily establish that the convex functions $\boldsymbol{\chi} \mapsto \pi_p^{\hom}(\mathbf{D},\boldsymbol{\chi})$ and $\mathbf{D} \mapsto \pi_p^{\hom}(\mathbf{D},\boldsymbol{\chi})$ are even. Therefore, they reach their minimum at zero. This means that we have:

$$\begin{aligned} \pi^{(N,0)}(\mathbf{D}) &= \inf_{\boldsymbol{\chi}} \pi_p^{\hom}(\mathbf{D},\boldsymbol{\chi}) = \pi_p^{\hom}(\mathbf{D},0) = \pi^N(\mathbf{D}) \\ \pi^{(0,M)}(\boldsymbol{\chi}) &= \inf_{\mathbf{D}} \pi_p^{\hom}(\mathbf{D},\boldsymbol{\chi}) = \pi_p^{\hom}(0,\boldsymbol{\chi}) = \pi^M(\boldsymbol{\chi}) \end{aligned} \tag{A.8}$$

6 Bibliography

Addessi, D., & Sacco, E. (2014). A kinematic enriched plane state formulation for the analysis of masonry panels. *European Journal of Mechanics - A/Solids*, *44*, 188–200. doi:10.1016/j.euromechsol.2013.10.013

Addessi, D., Sacco, E., & Paolone, A. (2010). Cosserat model for periodic masonry deduced by nonlinear homogenization. *European Journal of Mechanics - A/Solids*, *29*(4), 724–737. doi:10.1016/j.euromechsol.2010.03.001

Alpa, G., & Monetto, I. (1994). Microstructural model for dry block masonry walls with in-plane loading. *Journal of the Mechanics and Physics of Solids*, *42*(7), 1159–1175. doi:10.1016/0022-5096(94)90065-5

Anthoine, A. (1995). Derivation of the in-plane elastic characteristics of masonry through homogenization theory. *International Journal of Solids and Structures*, *32*(2), 137–163. doi:10.1016/0020-7683(94)00140-R

Anthoine, A. (1997). Homogenization of periodic masonry: Plane stress, Generalized plane strain or 3D modelling? *Communications in Numerical Methods in Engineering*, *13*(5), 319–326. doi:10.1002/(SICI)1099-0887(199705)13:5<319::AID-CNM55>3.0.CO;2-S

Bakhvalov, N., & Panasenko, G. (1989). Homogenisation: Averaging Processes in Periodic Media: Mathematical Problems in the Mechanics of Composite Materials. Springer.

Bensoussan, A., Lions, J.-L., & Papanicolaou, G. (1978). *Asymptotic analysis for periodic structures*. Amstredam-New York-Oxford: North-Holland Publishing Company.

Brencich, A., Corradi, C., & Gambarotta, L. (2008). Eccentrically loaded brickwork: Theoretical and experimental results. *Engineering Structures*, *30*(12), 3629–3643. doi:10.1016/j.engstruct.2008.05.010

Cecchi, A., & Sab, K. (2002). A multi-parameter homogenization study for modeling elastic masonry. *European Journal of Mechanics - A/Solids*, *21*(2), 249–268. doi:10.1016/S0997-7538(01)01195-0

Dallot, J., & Sab, K. (2008a). Limit analysis of multi-layered plates. Part I: The homogenized Love–Kirchhoff model. *Journal of the Mechanics and Physics of Solids*, *56*(2), 561–580. doi:10.1016/j.jmps.2007.05.005

Dallot, J., & Sab, K. (2008b). Limit analysis of multi-layered plates. Part II: Shear effects. *Journal of the Mechanics and Physics of Solids*, *56*(2), 581–612. doi:10.1016/j.jmps.2007.05.006

De Buhan, P., & de Felice, G. (1997). A homogenization approach to the ultimate strength of brick masonry. *Journal of the Mechanics and Physics of Solids*, *45*(7), 1085–1104. doi:10.1016/S0022-5096(97)00002-1

De Felice, G., Amorosi, A., & Malena, M. (2009). Elasto-plastic analysis of block structures through a homogenization method. *International Journal for Numerical and Analytical Methods in Geomechanics*, *34*(May 2009), 221–247. doi:10.1002/nag.799

Heyman, J. (1966). The stone skeleton. *International Journal of Solids and Structures*, *2*(2), 249–279. doi:10.1016/0020-7683(66)90018-7

Kourkoulis, S. K., & Ganniari-Papageorgiou, E. (2010). Experimental study of the size- and shape-effects of natural building stones. *Construction and Building Materials*, *24*(5), 803–810. doi:10.1016/j.conbuildmat.2009.10.027

Livesley, R. K. (1978). Limit analysis of structures formed from rigid blocks. *International Journal for Numerical Methods in Engineering*, *12*(12), 1853–1871. doi:10.1002/nme.1620121207

Lotfi, H. R., & Shing, P. B. (1991). An appraisal of smeared crack models for masonry shear wall analysis. *Computers & Structures*, *41*(3), 413–425. doi:10.1016/0045-7949(91)90134-8

Lourenço, P. B. (1996). Computational strategies for masonry structures. Delft University of Technology.

Lourenço, P. B., Milani, G., Tralli, A., & Zucchini, A. (2007). Analysis of masonry structures: review of and recent trends in homogenization techniquesThis article is one of a selection of papers published in this Special Issue on Masonry. *Canadian Journal of Civil Engineering*, *34*(11), 1443–1457. doi:10.1139/L07-097

Masiani, R., & Trovalusci, P. (1996). Cosserat and Cauchy materials as continuum models of brick masonry. *Meccanica*, *31*(4), 421–432. doi:10.1007/BF00429930

Massart, T. J., Peerlings, R. H. J., & Geers, M. G. D. (2007). An enhanced multi-scale approach for masonry wall computations with localization of damage. *International Journal for Numerical Methods in Engineering*, *69*(5), 1022–1059. doi:10.1002/nme.1799

Massart, T., Peerlings, R., Geers, M., & Gottcheiner, S. (2005). Mesoscopic modeling of failure in brick masonry accounting for three-dimensional effects. *Engineering Fracture Mechanics*, *72*(8), 1238–1253. doi:10.1016/j.engfracmech.2004.09.007

Milani, G., Lourenço, P. B., & Tralli, A. (2006a). Homogenised limit analysis of masonry walls, Part I: Failure surfaces. *Computers & Structures*, *84*(3-4), 166–180. doi:10.1016/j.compstruc.2005.09.005

Milani, G., Lourenço, P. B., & Tralli, A. (2006b). Homogenised limit analysis of masonry walls, Part I: Failure surfaces. *Computers & Structures*, *84*(3-4), 166–180. doi:10.1016/j.compstruc.2005.09.005

Milani, G., Lourenço, P. B., & Tralli, A. (2006c). Homogenised limit analysis of masonry walls, Part II: Structural examples. *Computers & Structures*, *84*(3-4), 181–195. doi:10.1016/j.compstruc.2005.09.004

Mistler, M., Anthoine, A., & Butenweg, C. (2007). In-plane and out-of-plane homogenisation of masonry. *Computers & Structures*, *85*(17-18), 1321–1330. doi:10.1016/j.compstruc.2006.08.087

Ottosen, N. (1977). A failure criterion for concrete. *Journal of the Engineering Mechanics Division, ASCE, 103*, 527–535.

Page, A. W. (1978). Finite element model for masonry. *Journal of the Structural Division, ASCE, 104*, 1267–1285.

Page, A. W. (1981). The biaxial compressive strength of brick masonry. *ICE Proceedings*, *71*(3), 893–906. doi:10.1680/iicep.1981.1825

Page, A. W. (1983). The strength of brick masonry under biaxial tension-compression. *International Journal of Masonry Construction, 3*, 26–31.

Pande, G. N., Liang, J. X., & Middleton, J. (1989). Equivalent elastic moduli for brick masonry. *Computers and Geotechnics*, *8*(3), 243–265. doi:10.1016/0266-352X(89)90045-1

Pau, A., & Trovalusci, P. (2012). Block masonry as equivalent micropolar continua: the role of relative rotations. *Acta Mechanica*, *223*(7), 1455–1471. doi:10.1007/s00707-012-0662-8

Pietruszczak, S., & Niu, X. (1992). A mathematical description of macroscopic behaviour of brick masonry. *International Journal of Solids and Structures*, *29*(5), 531–546. doi:10.1016/0020-7683(92)90052-U

Saada, A. S. (1974). *Elasticity: Theory and Applications*. New York, Toronto, Oxford, Sydney, Braunschweig: Pergamon Press Inc.

Sab, K. (2003). Yield design of thin periodic plates by a homogenization technique and an application to masonry walls. *Comptes Rendus Mécanique*, *331*(9), 641–646. doi:10.1016/S1631-0721(03)00144-X

Sahlaoui, R., Sab, K., & Heck, J.-V. (2011). Yield strength of masonry-like structures containing thin adhesive joints: 3D or 2D-interface model for the joints? *Comptes Rendus Mécanique, 339*(6), 432–438. doi:10.1016/j.crme.2011.03.018

Salençon, J. (1983). *Calcul à la Rupture et Analyse Limite*. Paris: Presses de l'Ecole Nationale des Ponts et Chaussées.

Salençon, J. (1990a). Introduction to the yield design theory and its applications to soil mechanics. *European Journal of Mechanics, A/Solids, 9*, 477–500.

Salençon, J. (1990b). Introduction to the yield design theory and its applications to soil mechanics. *European Journal of Mechanics, A/Solids, 9*, 477–500.

Salerno, G., & de Felice, G. (2009). Continuum modeling of periodic brickwork. *International Journal of Solids and Structures*, *46*(5), 1251–1267. doi:10.1016/j.ijsolstr.2008.10.034

Stefanou, I., Sulem, J., & Vardoulakis, I. (2008). Three-dimensional Cosserat homogenization of masonry structures: elasticity. *Acta Geotechnica*, *3*(1), 71–83. doi:10.1007/s11440-007-0051-y

Stefanou, I., Sulem, J., & Vardoulakis, I. (2010). Homogenization of interlocking masonry structures using a generalized differential expansion technique. *International Journal of Solids and Structures*, *47*(11-12), 1522–1536. doi:10.1016/j.ijsolstr.2010.02.011

Sulem, J., & Muhlhaus, H. (1997). A continuum model for periodic two-dimensional block structures. *MECHANICS OF COHESIVE-FRICTIONAL MATERIALS*, *2*, 31–46. doi:10.1002/(SICI)1099-1484(199701)2:1

Suquet, P. (1983). Limit Analysis and Homogenisation. *Comptes Rendus Mécanique*, *296*(5), 1355–1358.

Syrmakezis, C. A., & Asteris, P. G. (2001). Masonry Failure Criterion under Biaxial Stress State. *Journal of Materials in Civil Engineering*, *13*(1), 58–64. doi:10.1061/(ASCE)0899-1561(2001)13:1(58)

Trovalusci, P., & Pau, A. (2013). Derivation of microstructured continua from lattice systems via principle of virtual works: the case of masonry-like materials as micropolar, second gradient and classical continua. *Acta Mechanica*. doi:10.1007/s00707-013-0936-9

Zucchini, A., & Lourenço, P. B. (2002). A micro-mechanical model for the homogenisation of masonry. *International Journal of Solids and Structures*, *39*(12), 3233–3255. doi:10.1016/S0020-7683(02)00230-5

Zucchini, A., & Lourenço, P. B. (2004). A coupled homogenisation–damage model for masonry cracking. *Computers & Structures*, *82*(11-12), 917–929. doi:10.1016/j.compstruc.2004.02.020

Zucchini, A., & Lourenço, P. B. (2007). Mechanics of masonry in compression: Results from a homogenisation approach. *Computers & Structures*, *85*(3-4), 193–204. doi:10.1016/j.compstruc.2006.08.054